

## The *Spitzer*/GLIMPSE Surveys: A New View of the Milky Way

ED CHURCHWELL,<sup>1</sup> BRIAN L. BABLER,<sup>1</sup> MARILYN R. MEADE,<sup>1</sup> BARBARA A. WHITNEY,<sup>2</sup> ROBERT BENJAMIN,<sup>3</sup>  
 REMY INDEBETOUW,<sup>4</sup> CLAUDIA CYGANOWSKI,<sup>1</sup> THOMAS P. ROBITAILLE,<sup>5</sup> MATTHEW POVICH,<sup>1</sup>  
 CHRISTER WATSON,<sup>6</sup> AND STEVE BRACKER<sup>1</sup>

*Received 2008 September 20; accepted 2009 February 4; published 2009 March 12*

**ABSTRACT.** A brief description is given of the GLIMPSE surveys, including the areas surveyed, sensitivity limits, and products. The primary motivations for this review are to describe some of the main scientific results enabled by the GLIMPSE surveys and to note potential future applications of the GLIMPSE catalogs and images. In particular, we discuss contributions to our understanding of star formation and early evolution, the interstellar medium, galactic structure, and evolved stars. Infrared dark clouds (IRDCs), young stellar objects (YSOs), and infrared bubbles/H II regions are discussed in some detail. A probable triggered star formation associated with expanding infrared bubbles is briefly mentioned. The distribution and morphologies of dust and polycyclic aromatic hydrocarbons (PAHs) in the interstellar medium are discussed. Examples are shown from GLIMPSE images of bow shocks, pillars (elephant trunks), and instabilities in massive star-formation regions. The infrared extinction law of diffuse interstellar dust is discussed. The large-scale structure of the Galaxy has been traced by red-clump giants using the GLIMPSE point-source catalog to reveal the radius and orientation of the central bar, the stellar radial scale length, an obvious increase in star counts toward the tangency to the Scutum-Centaurus spiral arm, the lack of an obvious tangency from star counts toward the Sagittarius spiral arm, and a sharp increase in star counts toward the nuclear bulge. Recent results on evolved stars and some serendipitous discoveries are mentioned. More than 70 refereed papers have been published based on GLIMPSE data as of 2008 November.

*Online material:* color figures

### 1. THE SURVEYS

The *Spitzer Space Telescope* (Werner et al. 2004) Legacy program Galactic Legacy Infrared Mid-Plane Survey Extraordinaire (GLIMPSE) has provided a new view of our Galaxy that is leading to a deeper understanding of the physics of interstellar dust, star formation, and the large-scale structure of the Milky Way as traced by stars. Hallmarks of the Galactic disk at wavelengths from 3.6 to 24  $\mu\text{m}$  are H II regions/IR bubbles, young stellar objects (YSOs), massive star-formation regions, infrared dark clouds (IRDCs), diffuse dust and polycyclic aromatic hydrocarbon (PAH) emission, and tens of millions of stars. Because of its large areal coverage, GLIMPSE has revealed mid-infrared (MIR) features of large angular extent that have

not been recognized previously. An example is the large MIR bubble on whose periphery M17 lies. Povich et al. (2009) postulate that M17 may have been triggered by the expansion of this bubble when it collided with the M17 SW molecular cloud.

GLIMPSE consists of three separate surveys. GLIMPSE I fully imaged the Galactic plane from longitudes  $|l| = 10^\circ$  to  $65^\circ$  and latitudes  $|b| \leq 1^\circ$ , an area of 220  $\text{deg}^2$ , with a spatial resolution  $< 2''$  at wavelengths 3.6, 4.5, 5.8, and 8.0  $\mu\text{m}$  using the Infrared Array Camera (IRAC; Fazio et al. 2004). Each frame consisted of  $256 \times 256$  pixels each subtending  $1.2'' \times 1.2''$ . Each direction in the survey area was observed at least twice with an actual time per exposure of 1.2 s per exposure, providing  $3\sigma$  point-source sensitivity limits of 15.5, 15.0, 13.0, and 13.0 mag at 3.6, 4.5, 5.8, and 8.0  $\mu\text{m}$ , respectively. The saturation limits were 7.0, 6.5, 4.0, and 4.0 mag at 3.6, 4.5, 5.8, and 8.0  $\mu\text{m}$ , respectively. Both the detection limits and saturation limits depend on the point-source spatial density (i.e., confusion) and diffuse background brightness and spatial variation in complex ways that defy specification by a single parameter.<sup>7</sup> The background level for the sensitivity limits given

<sup>1</sup>Department of Astronomy, University of Wisconsin-Madison, Madison, WI 53706.

<sup>2</sup>Space Science Institute, Boulder, CO 80303.

<sup>3</sup>Department of Physics, University of Wisconsin-Whitewater, Whitewater, WI 53190.

<sup>4</sup>Astronomy Department, University of Virginia, Charlottesville, VA 22904-4325.

<sup>5</sup>School of Physics and Astronomy, University of St. Andrews, N. Haugh St. Andrews, Fife KY 169SS, Scotland, UK.

<sup>6</sup>Department of Physics, Manchester College Box 117, North Manchester, IN 46962.

<sup>7</sup>See the GLIMPSE Quality Assurance and Data Products documents at <http://www.astro.wisc.edu/sirtf/docs.html>.

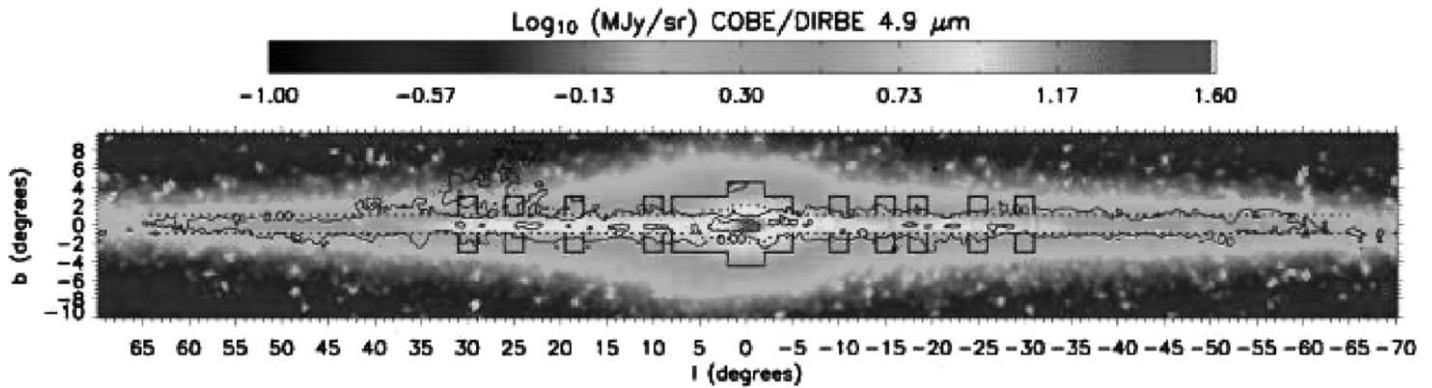


FIG. 1.—Area surveyed by the three GLIMPSE surveys superimposed on the COBE/DIRBE 4.9  $\mu\text{m}$  image. The scale bar at top is the intensity scale. Dotted line: the GLIMPSE I & II survey areas; Black solid line: the Galactic latitude extensions in the GLIMPSE 3D survey. See the electronic edition of the *PASP* for a color version of this figure.

above is  $<10$  MJy per star at 8  $\mu\text{m}$  (the *minimum* background level in the  $l = 284^\circ$  GLIMPSE validation area); for IRAC bands 1 and 2, this implies background levels very near 0 MJy per star. As shown in Figures 1 and 2 of the GLIMPSE Data Products v2.0 document,<sup>8</sup> the completeness limits gradually shift to brighter magnitudes with decreasing distance from the Galactic center due to increasing point-source surface density and average background brightness, but the detection limits do not vary significantly with Galactic longitude. The GLIMPSE I survey has cataloged 31,154,438 stars in its high reliability ( $\geq 99.5\%$ ) Point Source Catalog (GLMC) and 49,133,194 stars in its slightly lower reliability but more complete Point Source Archive (GLMA;  $\geq 5\sigma$ ).

GLIMPSE II fully imaged the inner  $20^\circ$  of the Galactic plane with the same resolution and sensitivity as that of GLIMPSE I. From  $|l| = 5^\circ$  to  $2^\circ$  degrees the latitude coverage was increased to  $b = \pm 1.5^\circ$  and from  $|l| = 2^\circ$  to  $0^\circ$  the latitude coverage was  $b = \pm 2^\circ$ . The latitude coverage was increased to obtain more coverage of the nuclear bulge. Each position on the sky was observed at least 3 times, twice at one epoch and once at a second epoch. A small region of about  $0.75^\circ \times 0.75^\circ$  centered on the Galactic center observed by S. Stolovy was included in our processing. The GLIMPSE II survey has cataloged 18,145,818 stars in its GLMC and 23,125,046 stars in its slightly lower reliability but more complete GLMA.

GLIMPSE 3D was designed to sample the latitude distribution of the central bar by extending the GLIMPSE I & II latitude coverage to  $\pm 3^\circ$  at nine selected latitudes and to  $\pm 4^\circ$  within  $2^\circ$  of the Galactic center. The GLIMPSE 3D survey has cataloged 20,403,915 stars in its GLMC and 32,214,210 stars in its slightly lower reliability but more complete GLMA. Not all GLIMPSE 3D source lists have been submitted to the Spitzer

Science Center (SSC) at this time; we expect all source lists to be submitted by the middle of 2009.

Figure 1 shows the entire region imaged in all three GLIMPSE surveys superimposed on the COBE/DIRBE 4.9  $\mu\text{m}$  color image. More than 440,000 individual  $5' \times 5'$  frames were observed to produce all three GLIMPSE surveys. Over a billion resolution elements were required to cover the entire survey. The total number of stars cataloged from the combined GLIMPSE surveys are 69,704,171 in the GLMC and 104,472,450 in the GLMA.<sup>9</sup>

In addition to the GLIMPSE data, the *Spitzer* Multiband Imaging Photometer (MIPS; Rieke et al. 2004) Galactic plane survey, referred to as MIPS GAL (Carey 2008) imaged the same area as the GLIMPSE surveys and has played an important role in interpreting the infrared properties of many of the objects detected in the GLIMPSE surveys, especially the 24  $\mu\text{m}$  data. Generally, when we refer to 24  $\mu\text{m}$  data, it should be understood to be from the MIPS GAL survey unless otherwise noted. The MIPS GAL images and catalogs are also archived at the Infrared Science Archive (IRSA).<sup>10</sup>

In the following, we will review some of the main contributions and new insights provided by the GLIMPSE surveys in combination with surveys at other wavelengths. The list of topics covered here are not exhaustive and reflect our own personal choices; other reviewers would likely make different choices.

<sup>9</sup> More details about the GLIMPSE surveys can be found at <http://www.astro.wisc.edu/sirtf/>. The GLMC and GLMA can be found at the following sites: <http://ssc.spitzer.caltech.edu/legacy/glimpsehistory.html> and the IRSA at <http://irsa.ipac.caltech.edu/data/SPITZER/GLIMPSE>.

<sup>10</sup> In addition, a web browser that permits a user to scan and zoom-in on any object in the entire survey false color images of GLIMPSE bands alone and a combined GLIMPSE plus MIPS GAL 24  $\mu\text{m}$  image is located at <http://www.alienearth.org/glimpse/>. This browser was developed by Dr. James Harold of Space Science Institute.

<sup>8</sup> The GLIMPSE Data Products v2.0 document is available online at [http://www.astro.wisc.edu/sirtf/glimpse1\\_dataproduct\\_v2.0.pdf](http://www.astro.wisc.edu/sirtf/glimpse1_dataproduct_v2.0.pdf).

## 2. STAR-FORMATION REGIONS

In this section, we will discuss star-formation regions from the earliest observed stages to advanced stages of evolution.

### 2.1. IRDCs and Star Formation

IRDCs are cold, dense, molecular or dust clouds seen at MIR wavelengths in silhouette against the MIR background emission. They are the cradle of star formation and the repository of molecular gas in the Galaxy. IRDCs represent the densest condensations in giant molecular clouds and are the most likely sites of future massive star formation. IRDCs were first identified in the Galactic plane by the *Infrared Space Observatory* (ISO; Kessler et al. 1996) and the *Midcourse Space Experiment* (MSX) satellite (Price et al. 2001) at mid-IR wavelengths. Carey et al. (1998), Egan et al. (1998), Hennebelle et al. (2001), and Redman et al. (2003) drew attention to the importance of these objects from MSX and ISO images. It was clear from the earliest detection of these objects that they are dense ( $>10^5 \text{ cm}^{-3}$ ), cold ( $<20 \text{ K}$ ), and the site of star formation (Carey et al. 1998; Pillai et al. 2006, 2007; and others). The GLIMPSE survey, because of its greater sensitivity ( $\sim 100$ ) and spatial resolution ( $\sim 10$ ) than MSX, has revealed a very large number of IRDCs and provided a more detailed picture of their morphologies, especially those with small angular sizes. IRDCs are most easily observed in the  $8 \mu\text{m}$  IRAC band because of the bright PAH emission that permeates the Galactic plane. Because they are seen in silhouette, we generally expect them to lie relatively close to us (i.e., their near kinematic distance); the contrast between background and IRDCs will be diminished for more distant IRDCs, especially in the inner Galaxy, and would be obscured by bright foreground PAH and thermal dust emission. No IRDCs so far studied in the GLIMPSE survey have been found to lie at the far distance (J. Jackson, private communication 2008). IRDCs are of special interest because they provide the raw material and conditions for initiation of star formation (Menten et al. 2005). In fact, at mid-IR wavelengths, YSOs in the act of forming are a common sight in IRDCs. See Bergin & Tafalla (2007) for an information-rich review of dark clouds in general including IRDCs.

#### 2.1.1. IRDC Morphologies

Many IRDCs are elongated with length-to-width ratios well in excess of 10:1. A typical example of a long filamentary IRDC seen in silhouette against diffuse  $8 \mu\text{m}$  background emission is shown in Figure 2. One IRDC filament (referred to by Jackson as “Nessie”) appears to extend over  $2^\circ$  in longitude ( $l \sim 336^\circ\text{--}334^\circ$ ); spectroscopy is needed to determine if this CO observations by J. Jackson and collaborators (private communication 2008) show that this cloud is a single dynamical structure. The elongated morphology of most IRDCs may be, at least in part, the result of contraction from a larger, less-dense state, which with conservation of angular momentum naturally

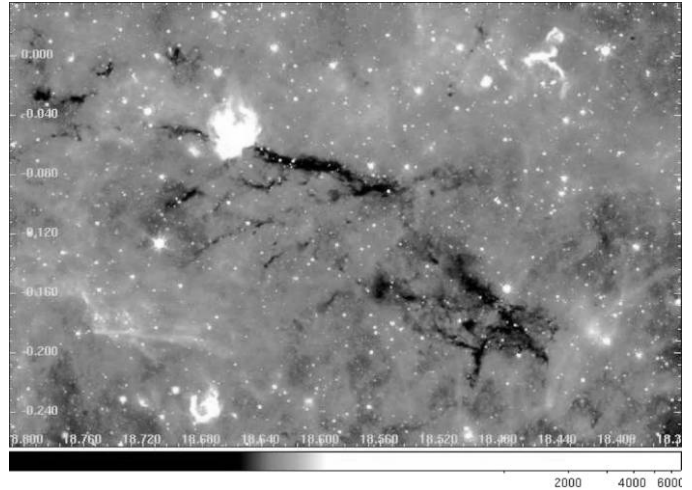


FIG. 2.—Example of a typical IRDC complex located at about  $l \sim 18.56$ ,  $b \sim -0.15$ . This is a monochromatic image at  $8 \mu\text{m}$  showing the morphology of IRDCs seen in silhouette. See the electronic edition of the *PASP* for a color version of this figure.

produces flattened structures. When viewed edge-on, these structures appear to be highly elongated. This scenario, however, cannot explain the nonplanar structures or wiggly filaments that are prevalent among IRDC morphologies. Differential Galactic rotation also tends to stretch large molecular clouds into linear structures, but this mechanism would only distort in the plane of the Galaxy leaving the wiggly filamentary structures unexplained. Perhaps the wiggles perpendicular to the plane are the result of a turbulent interstellar medium. The boundaries of IRDCs are generally not smooth. There are clearly smaller more opaque clumps within IRDCs. Might this possibly be an indication of gravitational fractionation? Further study will be needed to address this question.

A particularly nice example of YSOs (the bright  $24 \mu\text{m}$  spots) located along a filamentary IRDC is shown in Figure 3, but interestingly they seem to be isolated from each other and most of the volume of the IRDC appears to be quiescent with no star-formation activity. The high-resolution GLIMPSE images show that the central cores of many IRDCs are quite opaque at  $8 \mu\text{m}$ , indicating at least 3 mag of extinction or  $A_V \geq 70 \text{ mag}$  (Indebetouw et al. 2005). Of course, a few IRDCs that are less opaque at  $8 \mu\text{m}$  have been detected ( $A_{8m} \sim 0.5$  to 1 mag; Carey et al. 1998; Frieswijk et al. 2008). With typical extinctions  $A_V > 70 \text{ mag}$  and temperatures  $<20 \text{ K}$  (see § 3.3), it is difficult to understand why the entire volume of IRDCs does not collapse to produce stars. Clearly opaqueness at  $8 \mu\text{m}$  is not a sufficient condition for star formation.

#### 2.1.2. IRDC Radio Properties

IRDCs have been imaged in molecular lines of  $\text{NH}_3$  and/or  $\text{NH}_2\text{D}$  (Pillai et al. 2006, 2007; Sakai et al. 2008; Wang et al. 2008; and Devine et al. 2009); CO,  $^{13}\text{CO}$ , and/or  $\text{C}^{18}\text{O}$  (Pillai



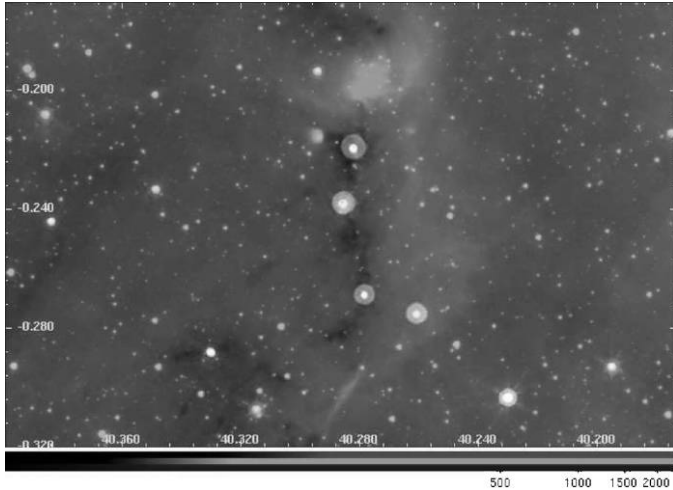


FIG. 3.—Example of an IRDC with a string of YSOs. The YSOs are shown as white spots, which are a combination of 8 and  $24\mu\text{m}$  emission. YSOs are brighter at  $24\mu\text{m}$  than at shorter wavelengths. See the electronic edition of the *PASP* for a color version of this figure.

et al. 2007; Ragan et al. 2006; Simon et al. 2006);  $\text{H}_2\text{CO}$  (Carey et al. 1998); CCS (Sakai et al. 2008; Devine et al. 2009);  $\text{N}_2\text{H}^+$  (Ragan et al. 2006; Sakai et al. 2008);  $\text{HC}_3\text{N}$  and isotopes (Pillai et al. 2007; Sakai et al. 2008);  $\text{CH}_3\text{OH}$  (Sakai et al. 2008); and probably others. The molecular lines show in some cases that more than one velocity component is present toward a given IRDC. All observations indicate that densities are high ranging from a few times  $10^3$  to  $10^6\text{ cm}^{-3}$  or greater and that temperatures are low, typically  $<20\text{ K}$  except toward a core in the process of star formation. Low temperatures were initially inferred by Carey et al. (1998) based on a deuterium fraction of 0.04 in the IRDC G79.34 + 033 from the  $\text{HDCO}/\text{H}_2\text{CO}$  intensities. Pillai et al. (2007) found that 60% of 32 IRDCs were detected in  $\text{NH}_2\text{D}$  and that  $\text{NH}_2\text{D}/\text{NH}_3$  ranged from 0.1 to 0.7; 0.7 is the highest degree of deuteration reported to date in the interstellar medium. Since deuteration only occurs in very cold environments, these data confirm that IRDCs are cold (typically  $\leq 20\text{ K}$ ). Rathborne et al. (2006) found from 1.2 mm continuum emission that the 38 IRDCs they observed have core masses ranging from 10 to  $2100 M_\odot$  and IRDCs as a whole have masses from 120 to  $16,000 M_\odot$  with a median of  $\sim 940 M_\odot$ ; they also report that the slope of the IRDC core mass spectrum is  $\sim 2.1 \pm 0.4$ , similar to the stellar initial mass function (IMF). The molecules that trace high densities show that all IRDCs have dense cores that are probably forming or soon will form a star(s). There is a close correlation of several dense molecular tracers and  $24\mu\text{m}$  point sources (Sakai et al. 2008 and Devine et al. 2009), especially  $\text{NH}_3$  and  $\text{CH}_3\text{OH}$ . As expected, the molecular distributions closely follow that of the  $8\mu\text{m}$  extinction boundaries, especially  $\text{NH}_3$  (Devine et al. 2009 and references therein). The radio data have provided critical velocity, column density, and excitation temperature distributions from

which volume densities, masses, and kinematic distances have been derived and confirmed the high densities and low temperatures inferred from IR images.

### 2.1.3. Extended Green Objects

In the early stages of producing the GLIMPSE image mosaics, it was discovered that there were a large number of extended objects that were especially bright in the  $4.5\mu\text{m}$  band of the IRAC detectors. These objects have been referred to by the GLIMPSE team as “green fuzzies” or extended green objects (EGOs) because the  $4.5\mu\text{m}$  band is commonly coded as green in false color images consisting of IRAC  $3.6\mu\text{m}$  (blue),  $4.5\mu\text{m}$  (green), and  $8.0\mu\text{m}$  (red) bands. Enhanced emission at  $4.5\mu\text{m}$  is believed to be due to shocked  $\text{H}_2(v=0-0)$  S(9, 10, 11) lines and/or  $\text{CO}(v=1-0)$  bandheads, all of which fall within the IRAC  $4.5\mu\text{m}$  band. Soon after their detection, it was hypothesized (Marston et al. 2004; Gutermuth et al. 2004; Noriega-Crespo et al. 2004; Rathborne et al. 2005; and possibly others) that EGOs are probably bipolar outflows from a central protostar; the outflows produce shocks when they crash into the ambient interstellar medium and excite NIR line emission. NIR  $\text{H}_2$  narrow-band images and *ISO* spectra show that the extended  $4.5\mu\text{m}$  emission of the massive DR21 outflow is due to shocked  $\text{H}_2$  (Davis et al. 2007; Smith et al. 2006, and references therein); Smith et al. (2006) do not detect CO lines in the *ISO* spectrum. While all IRAC bands contain  $\text{H}_2$  lines, modeling of protostellar jets predicts that the integrated  $\text{H}_2$  line luminosity is greatest in the  $4.5\mu\text{m}$  band (Smith & Rosen 2005).

Cyganowski et al. (2008) cataloged over 300 EGOs; an example is shown in Figure 4 (the bright  $24\mu\text{m}$  star [red] at the bottom edge of the green shell). The majority of cataloged EGOs are located toward IRDCs and, where the coverage of Class II 6.7 GHz  $\text{CH}_3\text{OH}$  maser surveys overlaps that of GLIMPSE I, EGOs and 6.7 GHz  $\text{CH}_3\text{OH}$  masers are strongly correlated (Cyganowski et al. 2008). Class II methanol masers are radiatively excited by IR photons from warm dust heated by the central accreting YSO (e.g., Cragg et al. 2005). The vast majority of EGOs have  $24\mu\text{m}$  counterparts in MIPS images. The poorer spatial resolution of MIPS ( $6''$  at  $24\mu\text{m}$ ), however, means that in many cases the  $24\mu\text{m}$  emission is confused, making it difficult to identify outflow-driving protostars from the MIR images alone (see Cyganowski et al. 2008). It is now believed that EGOs represent an early stage of star formation (the rapid accretion phase) when the infalling envelope is too opaque or the star too cool to excite large-scale PAH emission (which is bright at  $8\mu\text{m}$ ), allowing  $4.5\mu\text{m}$  emission to stand out. In Figure 5, the spectral energy distributions (SEDs) of two typical EGOs are shown. The MIR colors of EGOs are consistent with those of very young YSOs surrounded by substantial accreting envelopes (Cyganowski et al. 2008).

The catalog of Cyganowski et al. (2008) is not a complete catalog. It contains the most obvious examples of EGOs that show extended  $4.5\mu\text{m}$  excess emission and only those that

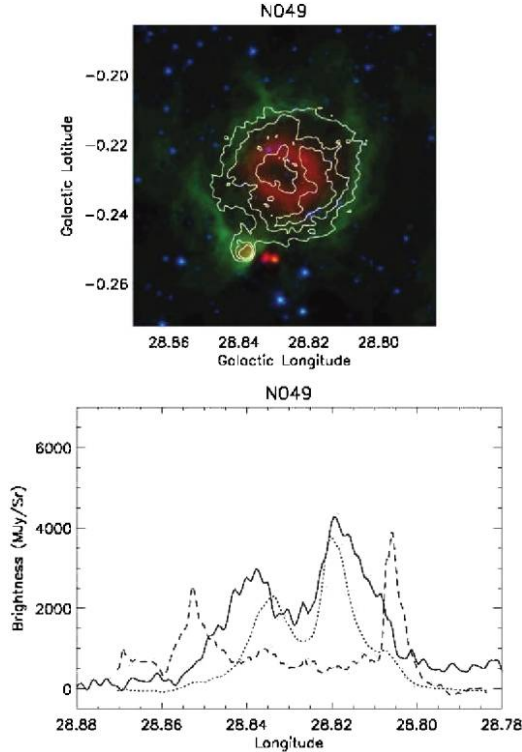


FIG. 4.—*Top*: 24  $\mu\text{m}$  (red), 8  $\mu\text{m}$  (green), 4.5  $\mu\text{m}$  (blue), and 20 cm (contours; Helfand et al. 2006) image of the IR bubble N49. YSOs are apparent on the bottom boundary of N49. The youngest ones are located in an IRDC; the IRDC may be difficult to recognize in the reproduced image but is quite clear in the original image. *Bottom*: slice in longitude through the center of N49. *Dashed line*: 8  $\mu\text{m}$  emission; *Dotted line*: 24  $\mu\text{m}$ ; *Solid line*: 20 cm. Note the central dip at 24  $\mu\text{m}$  and 20 cm that shows the wind evacuated by the central O5 star.

occur in the GLIMPSE I survey area (see also Yusef-Zadeh et al. 2007 for the Galactic Center region). The fact that EGOs stand out so clearly at 4.5  $\mu\text{m}$  in the IRAC bands provides an independent way of visually identifying a very early stage of massive star formation in the Galactic plane. The IR brightness of EGOs means that they can be detected at large distances in the disk of the Milky Way because they are almost extinction free at IRAC bands.

What is the evidence that EGOs trace *massive* star formation as opposed to the entire mass range of YSOs? EGOs cataloged in GLIMPSE are strongly correlated with 6.7 GHz Class II  $\text{CH}_3\text{OH}$  masers (Cyganowski et al. 2008), both tracers of early stages of massive star formation. Class II 6.7 GHz  $\text{CH}_3\text{OH}$  masers are *not* seen toward low-mass YSOs (Minier et al. 2003) but are ubiquitous toward massive YSOs (Szymczak et al. 2005; Ellingsen 2006, 2007). The close association of Class II 6.7 GHz  $\text{CH}_3\text{OH}$  masers and EGOs—shown in Cyganowski et al. (2008) using the high-angular-resolution maser surveys of Ellingsen (2006), Walsh et al. (1998), and Caswell (1996)—strongly implicate massive YSOs. The range of distances to EGOs with kinematic distances from associated 6.7 GHz  $\text{CH}_3\text{OH}$  masers—2.6 to 5.3 kpc—is also typical of distances to

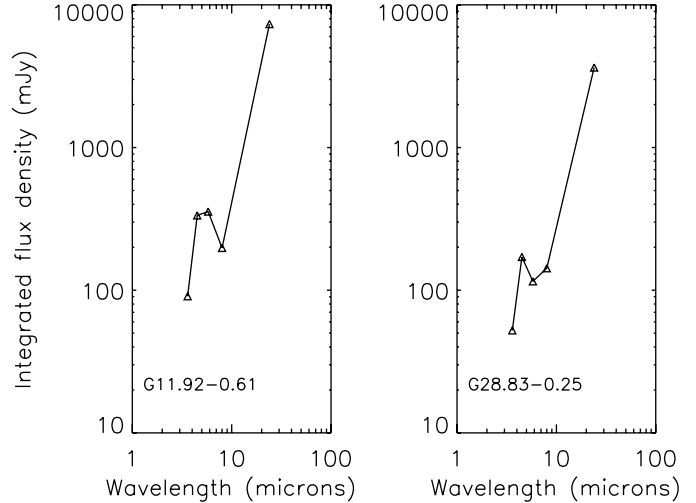


FIG. 5.—Example SEDs of two EGOs. Note the excess emission at 4.5 and sometimes at 5.8  $\mu\text{m}$  as well.

massive star-formation regions in the Galactic Plane (see Cyganowski et al. 2008). In addition, while extended 4.5  $\mu\text{m}$  emission can be associated with low-mass outflows (e.g., HH46/47, Noriega-Crespo et al. 2004; Velusamy et al. 2007), GLIMPSE is a shallow survey. The faintest EGOs cataloged by Cyganowski et al. (2008) have surface brightnesses at 4.5  $\mu\text{m}$  at least twice those of the bright knots in the HH46/47 outflow (see Cyganowski et al. 2008). It is unlikely that the relatively faint extended 4.5  $\mu\text{m}$  emission, seen in low-mass star-forming regions would have been detected in the search for EGOs in the GLIMPSE images.

## 2.2. YSOs in the GLIMPSE Survey

Examination of the GLIMPSE/MIPSGAL survey images emphatically illustrates that in the neighborhood of YSOs and hot stars (especially O and early B stars that ionize H II regions) the associated dust becomes a bright beacon in the infrared. One can easily pick out the massive star-formation regions from their brightness at wavelengths  $\geq 5.8 \mu\text{m}$ , especially at 24  $\mu\text{m}$ . These regions illuminate the young stellar population in the Milky Way by extended emission from PAH bands, thermal dust emission, and stochastic emission from very small grains (VSGs) that are transiently heated by absorption of single stellar UV photons and rapidly cool by radiating the excess heat away at infrared wavelengths (Draine 2003). As mentioned in § 2.1.3, YSOs are quite apparent throughout the GLIMPSE survey, especially by their emission at 8  $\mu\text{m}$  (due to thermal dust and/or PAH emission) and 24  $\mu\text{m}$  (a combination of thermal and stochastic emission). A good example of YSOs is shown in Figure 3, where a string of YSOs are seen against the darkness of their natal IRDC.

A search of the GLIMPSE GLMC for very red stars  $[K] - [8.0] > 3$  identified  $\sim 45,000$  stars. It was found that these



generally tend to be concentrated toward IRDCs as illustrated in Figure 6. What are these very red stars? There are several possibilities: normal stars reddened by a foreground IRDC, YSOs, asymptotic giant branch (AGB) stars, and background galaxies. Because GLIMPSE was a shallow survey, it was barely sensitive enough to detect only a few of the nearest brightest galaxies, so we can safely exclude galaxies. In addition, galaxies detected in the GLIMPSE surveys are extended and easily distinguished from stars. In fact, the SEDs of most of the very red point sources were fit with reddened stellar photospheres. Robitaille et al. (2008) have characterized more than 19,000 IR emission sources in the GLMC using a selection criteria of  $[4.5] - [8.0] > 1$  and strict brightness and quality criteria. Since the mid-IR extinction law is relatively flat at  $[4.5] - [8.0]$  (Indebetouw et al. 2005 and others; see § 3.3), a large value of this color is due to infrared emission rather than dust extinction. Using color selections that reasonably separate YSOs from AGB stars (with some overlap, however), Robitaille et al. (2008) found that  $\sim 60\%$  ( $> 11,000$ ) of the red sources are YSOs and  $\sim 40\%$  are AGB stars. This is certainly an underestimate of the total number of YSOs in the survey area because the stringent selection criteria used for inclusion rules out many probable YSOs, and the use of the GLMC rules out many YSOs

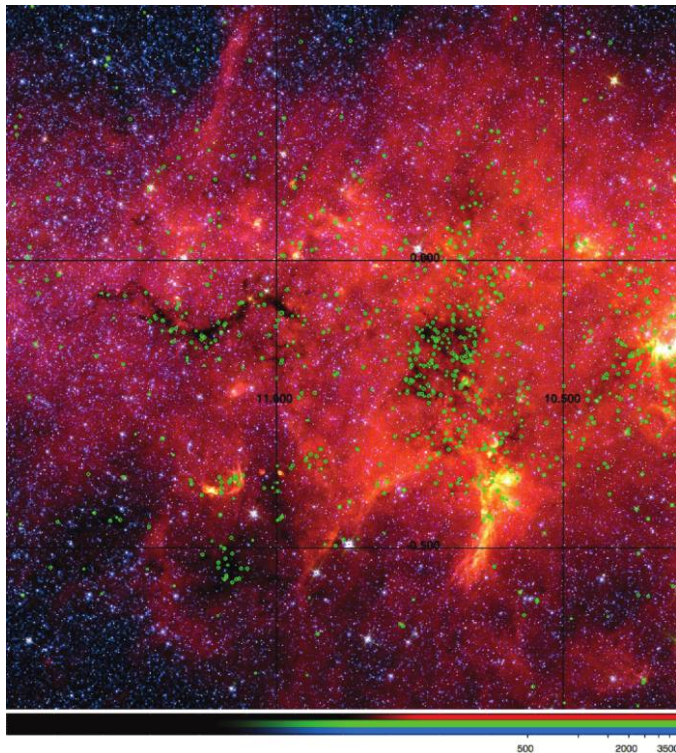


FIG. 6.—GLIMPSE image (red: 8  $\mu\text{m}$ ; green: 5.8  $\mu\text{m}$ ; blue: 3.6  $\mu\text{m}$ ) showing the locations of very red stars ( $K - [8] > 3$ ) designated by green circles. Note the clustering toward IRDCs of the green circled stars.

that are not point sources. The YSOs were found to have a clumpy distribution in the Galaxy (Fig. 7, *bottom*), whereas the AGB stars are smoothly distributed in the disk, as shown in Figure 7 (*top*). They also found that over 70% of the “extreme” AGB stars identified within  $10^\circ$  of the Galactic center are variable (this region of the survey had two separate epochs of observing, allowing the study of variability).

The GLIMPSE/MIPSGAL surveys provide the possibility to identify a substantial fraction of the YSO population in the inner Galaxy, especially those objects destined to become O and B stars, and presents an opportunity to redetermine the current global star-formation rate by directly counting YSOs. The distances at which YSOs can be detected in the GLIMPSE surveys depends on background brightness, the evolutionary state of the YSO, and other parameters. Robitaille et al. (2008) plot the range of distances at which Stage I and II YSOs would be detectable in the GLIMPSE surveys (see their Fig. 18). The *average* distance at which a 1000  $L_\odot$  (bolometric) Stage I YSO can be detected in the GLIMPSE survey is  $\geq 2$  kpc and a Stage II  $10^3 L_\odot$  YSO is  $\geq 6$  kpc. More luminous YSOs, of course, can be detected at greater distances. One reason the star-formation rate is of interest is that the *Spitzer* data has shown that star formation appears to extend well beyond the central cores of massive star-formation regions and young clusters. In these extended regions distributed star formation appears to be occurring (i.e., well outside the traditionally recognized cores of young clusters; see Whitney et al. 2004b; Megeath et al. 2004; Gutermuth et al. 2004; Muzerolle et al. 2004; Gutermuth et al. 2005; Indebetouw et al. 2007; Povich et al. 2009; Allen et al. 2007; Gutermuth et al. 2008; and others). Efforts are proceeding to reevaluate the global star-formation rate in the Galaxy to determine if this newly recognized component of star formation significantly contributes to the canonical star-formation rate of  $0.8\text{--}13 M_\odot \text{yr}^{-1}$  with a most likely value of  $3 M_\odot \text{yr}^{-1}$  (Cox 2000).

To help analyze the large population of YSOs observed by *Spitzer* in the GLIMPSE survey, Robitaille et al. (2006) computed a grid of 200,000 SED models of YSOs using the 2D, Monte Carlo radiation transfer code of Whitney et al. (2003a, 2003b, 2004a). Robitaille et al. (2007) developed a linear regression tool to select model SEDs that agree with observations to within a specified  $\chi^2$ , first demonstrated by Indebetouw et al. (2007) in the M16 massive star-formation region. The range of model parameters corresponding to the well-fit SEDs shows how well they are constrained. Some model parameters are better constrained than others, depending on, for example, the wavelength range of the data and the evolutionary stage of the source. SED-fitting, as opposed to color-color analysis, allows physical properties such as stellar mass, temperature, luminosity, envelope accretion rate, and disk mass to be estimated for the YSOs, and shows if the properties are well determined or not based on their ranges. Following the spirit of the Legacy program concept, the transfer codes, grid

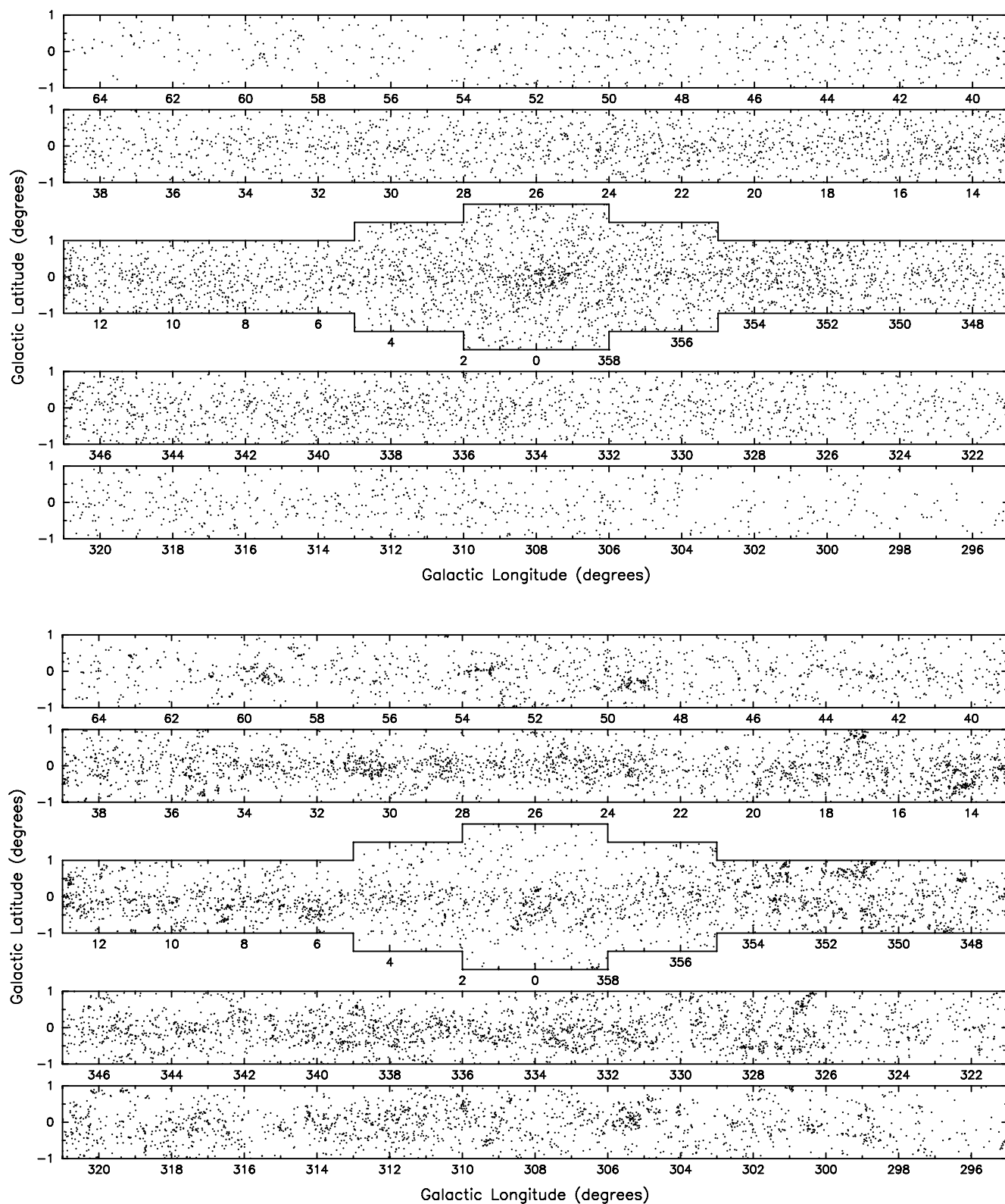


FIG. 7.—Spatial distribution of all the AGB candidates identified in the GLIMPSE survey (*top*) and YSO candidates (*bottom*). Image from Robitaille et al. (2008).

of models, and fitting tool are publicly available.<sup>11</sup> These tools have been used to find evidence for ongoing massive star formation in RCW 49 (Whitney et al. 2004b), the distribution of stellar masses of YSOs in the G34 region (Shepherd et al. 2007), separate YSOs from AGBs, estimate the star-formation rate in an extended region around M17 (Povich et al. 2007, 2009), and find YSOs in regions surrounding IR bubbles (Watson et al. 2008). Watson et al. (2008) also developed a method to identify the central ionizing sources by fitting their SEDs (2MASS + IRAC) with stellar photospheres. The SED-fitting results are degenerate in  $T_*$  and  $A_V$ . If the star is assumed to be at the distance of the bubble, its radius can be computed and the  $T_* - R$  dependence on spectral type can be compared to those of established spectral types. The intersection of the computed  $T_* - R$  curve with that for stellar spectral types computed from model atmospheres can determine the spectral type of the ionizing star. This method was confirmed by optical spectroscopy of selected stars toward several IR bubbles (Watson et al. 2008). Studies are continuing to determine properties of YSOs in several individual star-forming regions, and a larger-scale model of YSOs distributed throughout the Galaxy is planned for comparison with the infrared catalog of Robitaille et al. (2008).

Uzpen et al. (2005, 2007) have made a concerted effort to identify circumstellar matter around main-sequence stars from an analysis of their MIR excess emission. Uzpen et al. (2005) searched for  $\beta$  Pic analogs toward the RCW49 star-formation region by identifying  $8\ \mu\text{m}$  excess emission. They identified 33  $8\ \mu\text{m}$  excess sources, 18 of which they concluded are consistent with circumstellar debris disks. Uzpen et al. (2007) extended their search for  $\beta$  Pic analogs toward 230 Tycho-2 Spectral Catalog stars. Of these 14 appear to have IR luminosities and temperatures consistent with  $\beta$  Pic debris disk systems or Class II pre-main-sequence systems.

### 2.3. IR Bubbles/H II Regions

IR bubbles are arguably the most spectacular objects in the GLIMPSE/MIPSGAL images. Churchwell et al. (2006; 2007) have cataloged almost 600 bubbles in the GLIMPSE I & II areas. Most of the *luminous* ones coincide with radio H II regions, indicating that they are produced by radiation and winds of O and early B stars. They represent O and B stars at ages typically  $\sim 10^6$  yr. The Churchwell et al. catalogs make no claim for completeness; they are simply a list of the most prominent ones. The GLIMPSE I survey area is known to be especially incomplete for bubbles with very small ( $\leq 1'$ ) and very large ( $> 30'$ ) angular diameters. Figure 4 shows a typical IR bubble produced primarily by a single O5 star; this is N49 in the Churchwell et al. (2006) catalog. Figure 8 (RCW 49) is an example of a very different IR bubble; it is produced by a luminous

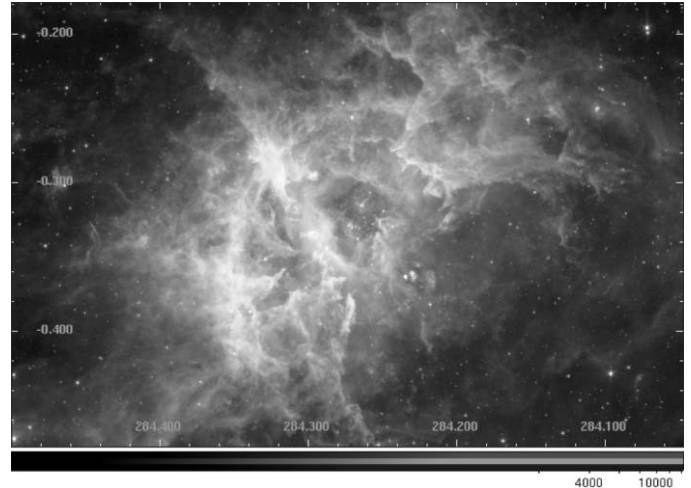


FIG. 8.—Image of the bubble blown by the luminous star cluster Westerlund 2. This image combines 8, 5.8, and  $3.6\ \mu\text{m}$  IRAC bands. The labels are galactic coordinates in degrees. The central cavity, multiple pillars (elephant trunks), the Wes2 cluster, and a bow shock (lower right) are easily identifiable in this image. See the electronic edition of the *PASP* for a color version of this figure.

star cluster (Westerlund 2) plus two WR stars that lie outside the central cluster. Figures 4 and 8 show bubbles with very different morphologies and physical properties.

#### 2.3.1. Statistical Properties

About 38% of the MIR bubbles in the Churchwell et al. (2006, 2007) catalogs do not have complete rings; that is, it appears that the swept-up shells have been blown out presumably in the direction where the confining shell is least dense; the bubbles shown in Figure 8 is an example of this phenomenon. The bubbles are fairly eccentric;  $\sim 65\%$  have eccentricities between 0.55 and 0.85 with a peak in the distribution at  $\sim 0.65$ . Departure from sphericity is probably produced by the ambient density distribution of the ISM; possible focusing mechanisms of the stellar wind and radiation, such as an accretion disk, may also play a role, especially in the earliest period of expansion. Winds from O stars, as opposed to bipolar outflows, are expected to be basically spherical (Lamers & Cassinelli 1999). We have not been able to relate bubble shape with the presence or absence of a circumstellar disk. Most bubbles have small angular diameters; almost 90% are smaller than  $4'$ . Over 85% of the bubbles have shell thicknesses  $< 1'$ , and the average shell thickness increases linearly with shell radius in agreement with predictions for windblown bubbles (Weaver et al. 1977). The bubbles are tightly concentrated to the Galactic plane; their angular scale height is  $\sim 0.63^\circ \pm 0.03^\circ$ . The projected distribution of MIR bubbles is similar to that of O and B stars in the Galaxy. The surface density of bubbles is  $\sim 5\ \text{deg}^{-2}$  in the GLIMPSE II survey area and reduces to  $\geq 1.5\ \text{deg}^{-2}$  in the GLIMPSE I survey area. Their distribution in the projected Galactic plane is essentially identical to that of O and B stars.

<sup>11</sup> See <http://www.astro.wisc.edu/protostars>.



### 2.3.2. MIR Radiation Properties

One of the key new insights revealed by the *Spitzer* GLIMPSE/MIPSGAL images is the role of dust in H II regions and their photodissociation regions (PDRs). The combination of IRAC, MIPS, and high-resolution radio continuum data show that H II regions are surrounded by a bright  $8\ \mu\text{m}$  shell that traces the PDR associated with each H II region. Inside the  $8\ \mu\text{m}$  shell, thermal dust emission dominates (especially at  $24\ \mu\text{m}$ ). Radio continuum and  $24\ \mu\text{m}$  emission are essentially coincident with each other, proving that dust is present within H II regions. In addition, the radio continuum clearly terminates very close to the inner face of the  $8\ \mu\text{m}$  shell, indicating that H II regions are confined by their PDRs (see Watson et al. 2008). Figures 4 and 9 are good examples of this morphology. In H II regions blown by stellar winds, the immediate volume

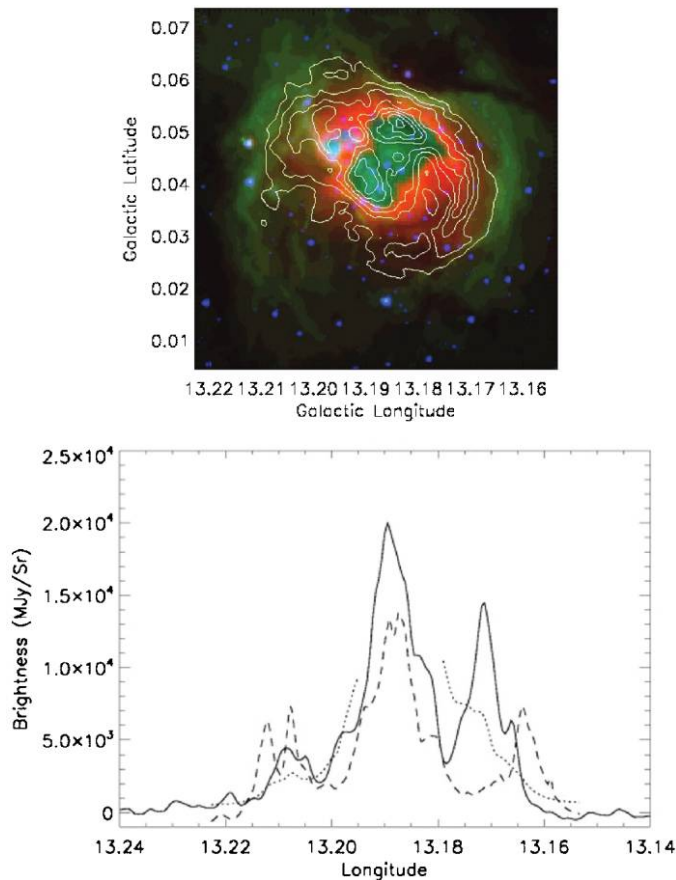


FIG. 9.—*Top*: GLIMPSE image of the IR bubble N010 (Churchwell et al. 2006). The color coding is the same as in Fig. 4 and the contours are 20 cm continuum (Helfand et al. 2006). The dark green at the center represents saturated  $24\ \mu\text{m}$  emission. *Bottom*: A slice through the approximate center of the bubble in longitude. *Solid line*: 20 cm continuum magnified by  $10^6$ ; *dashed line*:  $8\ \mu\text{m}$  emission magnified by a factor of 5; *dotted line*:  $24\ \mu\text{m}$  emission with no magnification. At the center,  $24\ \mu\text{m}$  emission is saturated (not plotted) and both  $8\ \mu\text{m}$  and 20 cm emission peak. This peak is in contrast to the relative distributions in N49 (Fig. 4) where none of the tracers peak at the center.

around the star is basically evacuated of both gas and dust producing a “dip” in  $24\ \mu\text{m}$  and radio continuum brightness toward N49 (Fig. 4); neither is there any evidence for  $8\ \mu\text{m}$  (PAH) emission inside the  $8\ \mu\text{m}$  shell because PAHs are destroyed by the stellar UV radiation (see Watson et al. 2008; Povich et al. 2007). In H II regions ionized by late O stars or cooler,  $8\ \mu\text{m}$ ,  $24\ \mu\text{m}$ , and radio continuum all peak at the location of the ionizing star(s) (Fig. 9). This situation is different from bubbles dominated by stellar winds where all tracers either have a dip at the central star or are absent altogether at the center. The IR emission at the center of N010 is due to thermal dust and stochastic dust emission produced by absorption of single UV photons that briefly heat VSGs, which subsequently cool by emitting IR radiation. There are no strong nebular lines in the MIPS  $24\ \mu\text{m}$  band; *Spitzer*/IRS spectra currently being prepared for publication confirm this. The PAH destruction radius coincides rather precisely with the H II region ionization front.

The above morphology has some important implications. The fact that dust seems to be well mixed within the  $\text{H}^+$  gas implies that: (1) H II regions are older than their dynamical ages would imply (i.e., their radii are smaller at a given age than they would be in the absence of dust); (2) the lifetimes of dust in the hostile environments of hot stars must either be  $\geq 10^6$  yr (the minimum age of several well-studied H II regions) or the dust must be continuously replenished; and (3) because dust in these environments is highly positively charged, the dust becomes the dominant coolant. Churchwell and Everett (2008) have studied these effects in some detail in N49, shown in Figure 4.

### 2.3.3. Triggered Star Formation

Triggered star formation is another topic that has come to the fore with the GLIMPSE/MIPSGAL images. Churchwell et al. (2006, 2007) identified YSOs on the periphery of or superimposed on expanding H II regions or dust bubbles. In a catalog of almost 600 bubbles, YSOs were found toward about 13%. Although positional coincidences are not a proof of triggering, it is certainly suggestive that these YSOs have been triggered by compression of swept-up or preexisting molecular clumps due to expansion of the H II regions. Deharveng et al. (2005) and Watson et al. (2008) have studied several H II regions and reinforced that triggered star formation indeed appears to be occurring toward some expanding H II regions, although Watson et al. (2008) do not find a significant increase of YSOs toward the PDRs of H II regions, indicating that this mechanism of star formation is not a major formation mechanism. Figure 4 (N49) is an H II region and/or IR bubble that appears to have triggered three YSOs each in somewhat different stages of evolution. The one at bottom right is a bright  $24\ \mu\text{m}$  source but does not have the  $4.5\ \mu\text{m}$  bow tie characteristic of EGOs; the one to the left of the  $24\ \mu\text{m}$  source is bright at both  $24$  and  $4.5\ \mu\text{m}$  and is a classic example of an EGO; and, the bright source(s) to the left of the EGO is bright at all wavelengths including 20 cm radio continuum. We hypothesize that the rightmost source is either

a lower-mass YSO that does not produce excess emission at  $4.5\ \mu\text{m}$ , or it is too obscured by an opaque envelope, or the outflow is too small to be detectable by *Spitzer*. At the distance of N49 (5.7 kpc), an outflow with a velocity of  $50\text{--}100\ \text{km s}^{-1}$  would require 540 to 270 yr to achieve a radial distance from the central protostar of 2 pixels ( $2.4''$ ). The middle source clearly has the extended  $4.5\ \mu\text{m}$  emission believed to trace the bipolar outflow from a YSO. The leftmost source(s) have had time to produce both a detectable H II region and a small IR bubble, both of which indicate a more advanced age than the other two sources to its right. If this hypothesis is correct, it indicates that the time between these early stages of evolution must be very short because all of this must have occurred within a few times  $10^5$  yr. This is consistent with predicted timescales for the evolution of massive stars.

### 2.3.4. Star Clusters

Mercer et al. (2005) developed an automated algorithm to identify star clusters based on increased stellar surface density relative to the local average surface density. They detected 59 new stellar clusters using this search algorithm. An additional 33 were found by visual inspection. The automated search algorithm did not work as well as hoped mostly due to the bright variable background.

## 3. THE INTERSTELLAR MEDIUM

In addition to IRDCs and H II regions, the GLIMPSE surveys have highlighted the wide distribution of interstellar dust along with PAHs and VSGs in the ISM, as well as bow shocks, pillars (elephant trunks), and instabilities in massive star-formation regions.

### 3.1. Dust and PAHs in the ISM

The GLIMPSE images of the Galactic disk vividly demonstrate that interstellar dust and PAHs are not distributed smoothly or uniformly. At resolutions  $<2''$  arc, interstellar dust is clearly distributed in fine, wispy filaments. Even in the dense bright PDR shells surrounding H II regions, PAHs are filamentary with little or nothing between the filaments, indicating that the ISM, and even dense PDR shells, are mostly empty. This has important implications for the propagation of radiation from stars, especially O and B stars, and the ISM because in a clumpy or filamentary or sheetlike medium, the mean free path length of photons is substantially greater than that in a uniform medium. Most soft UV photons ( $\lambda > 912\ \text{\AA}$ ) that can pass through the ionization fronts of H II regions, and planetary nebulae can travel substantially farther into the ISM and excite PAHs and raise the ionization fractions of metals over a large fraction of the ISM, thus explaining the wide distribution of  $8\ \mu\text{m}$  (PAH) and warm dust emission at  $24\ \mu\text{m}$  in the Galactic plane. In a filamentary medium, the concept of an ionization “front” also is likely to be rather porous resulting in boundaries between

$\text{H}^+$ ,  $\text{H}^0$ , and  $\text{H}_2$  that are less sharp (i.e. thicker) than predicted by models that assume uniform density distributions. At distances well away from bubbles, the IR colors of the diffuse ISM are relatively uniform, providing independent support for a porous ISM.

Heitsch et al. (2007) produced model images of molecular clouds bathed in the radiation field of a nearby O star to help answer the question of whether the GLIMPSE diffuse emission structures can be interpreted as density enhancements. They found that as the density of material (and therefore optical depths) increased, shadowing and irradiation effects can completely alter the appearance of an object. However, in the more diffuse regime [ $n(\text{HI}) \lesssim 100\ \text{cm}^{-3}$ ], flux density maps may be used to trace the 3D density structure of the cloud via density gradients. Thus, while caution is in order, GLIMPSE can provide quantitative insight into the turbulent structure of the interstellar medium. Bethell et al. (2007) have modeled radiative transfer of UV radiation through a clumpy molecular cloud and shown that UV radiation can penetrate, and therefore alter ionization conditions, 2–3 times deeper into a clumpy cloud than into a uniform density cloud.

Even at MIR wavelengths, some large molecular clouds have high enough opacities that background stars are attenuated. In Figure 10, the number of stars in the GLMC per  $0.1\ \text{deg}^2$  is plotted as a function of galactic position. In the inner part of the Galaxy where the number of stars is high, one can easily see the outline of major molecular clouds and massive star-formation regions by the decrease in the number of stars at these locations (indicated in Fig. 10). Some of the well-known clouds are noted in Figure 10, among which are M16, M17, W31, W33, and W43. By modeling the spectral energy distributions of the stars seen toward these clouds, it is possible to estimate their optical depths from which masses can be inferred (Whittet 1992), providing an important independent check on radio determinations.

### 3.2. Bow Shocks, Pillars, and Instabilities

In massive star-formation regions (MSFRs) where numerous, still accreting YSOs are in close proximity with each other, one should expect to find bow shocks produced by YSO outflows and hot star winds crashing into each other and into the ambient ISM. Indeed, in the GLIMPSE images of MSFRs, several bow shocks have been reported by Povich et al. (2008). In Figure 11, a montage of six proposed bow shocks are shown in M17 and RCW49. The bow shocks stand out at MIR wavelengths due to higher densities produced by shock compression and to high dust temperatures due to heating mostly by stellar radiation. See Povich et al. (2008) for further details and the electronic edition for a color version where the bow shocks are more apparent.

Pillars and instabilities are ubiquitous at the inner faces of and within PDR regions around H II regions and massive star clusters. Good examples of both are seen in M16 (the “fingers



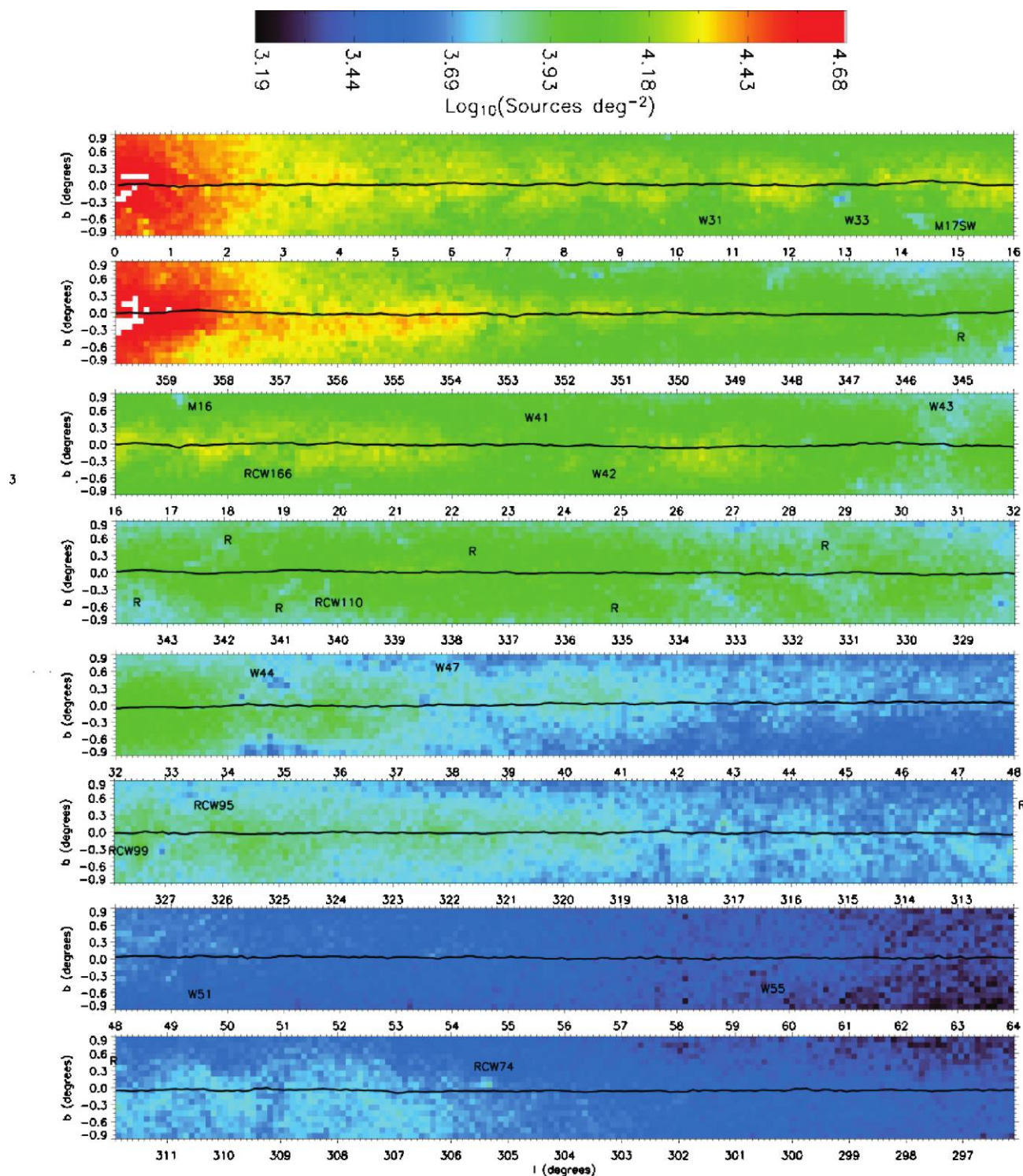


FIG. 10.—Log of the number of sources per  $\text{deg}^2$  from the GLMC at  $4.5 \mu\text{m}$  in the magnitude range 6.5–12.5. The Galactic longitude is labeled below each strip and each pair of strips represent equal segments of the plane on opposite sides of the Galactic center. Note the systematic decrease in the number of sources with distance from the center, the asymmetry in the number of sources in the first quadrant vs. that in the fourth quadrant at  $|l| < 30^\circ$ , the decrease in star counts at locations of known major molecular clouds, and the very small deviations in latitude of the stellar midplane indicated by the horizontal solid line (see Benjamin et al. 2005).



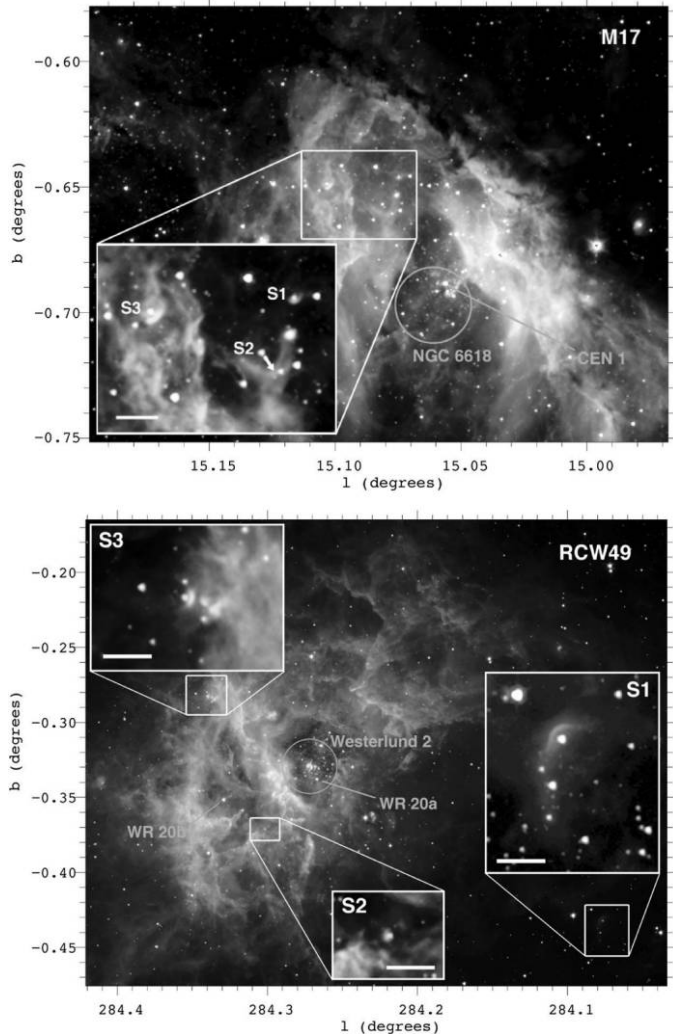


FIG. 11.—*Top panel:* GLIMPSE image of M17 ( $3.6\ \mu\text{m}$ ,  $4.5\ \mu\text{m}$ ,  $5.8\ \mu\text{m}$ ,  $8\ \mu\text{m}$ ). Zoomed images of three proposed bow shocks are shown in the insets. The scalebar is  $30'' = 0.23\ \text{pc}$  at a distance of  $1.6\ \text{kpc}$  (see Povich et al. 2008). *Bottom panel:* image of RCW49 (same scheme as top panel) showing zoomed image insets of three proposed bow shocks in this massive star-formation region (Povich et al. 2008). See the electronic edition of the *PASP* for a color version of this figure.

of creation” made famous by the *HST* images are also seen in emission in GLIMPSE; see Indebetouw et al. 2005) and in RCW49 (Fig. 8). The inner face of the outer shell around the Westerlund 2 (a luminous, massive star cluster) has been badly eroded by the action of stellar radiation and stellar winds. Here, pillars of higher-density gas and dust protrude inward toward the star cluster with obvious bright, shocked surfaces at the head or tip of the pillars. In this MSFR, we are seeing the process of mass clearing of the natal cloud by the action of stellar winds and radiation from Westerlund 2 and the two WR stars (WR20a, b) located within the RCW49 complex. Churchwell et al. (2004) and Whitney et al. (2004b) have discussed the diffuse emission and stellar populations, respectively, in this re-

gion. Churchwell et al. (2004) pointed out in their Figure 1 a bright, thin, wiggly feature that they suggested might be an example of a “Vishniac” instability. This is an instability that occurs when a sheet of gas is compressed from both sides and with time develops instabilities that cause the sheet to become wrinkled—when seen edge-on these instabilities will look like a thin wiggly feature. It has not been proven that this feature is, in fact, a Vishniac instability, but it might be well worth the time of a dynamicist to attempt a hydrodynamic model of this feature.

### 3.3. Infrared Extinction Law

Lutz et al. (1996) used *ISO* spectral line observations to derive the diffuse interstellar infrared extinction law. They used H-recombination lines that lie in the wavelength range  $2.5\text{--}9\ \mu\text{m}$  and found that  $A_\lambda/A_V$  is essentially constant from about  $4\ \mu\text{m}$  to about  $8\ \mu\text{m}$  toward the Galactic Center. This result was confirmed by Indebetouw et al. (2005) using an entirely different technique based on GLIMPSE stellar photometry. Indebetouw et al. (2005) were able to identify along three different lines of sight red-clump giants (RCGs), which have a narrow range of intrinsic luminosities and colors. Using RCGs, they also found that the diffuse interstellar medium differential reddening and extinction from  $\sim 4$  to  $8\ \mu\text{m}$  is constant in contrast to theoretical expectations. Roman-Zúñiga et al. (2007) investigated the  $1.25\text{--}7.76\ \mu\text{m}$  extinction law in the star-forming dark cloud B59 and found that it deviates only slightly from that of Indebetouw et al. (2005), but  $R_V = 5.5$  and larger grains were more consistent for B59 grains than for ISM grains. Ganesh et al. (2008) used red-clump giants at  $l = -45^\circ$ ,  $b = 0.0^\circ$ , using data from *ISO*, GLIMPSE, and 2MASS to examine the MIR extinction law and found a relation consistent with Indebetouw et al. (2005). Jiang et al. (2003) examined an  $\sim 0.1\ \text{deg}^2$  area centered at  $l = -18.63^\circ$ ,  $b = 0.35^\circ$ , using ISOGAL and DENIS data to derive  $A_{7\mu\text{m}}/A_V \sim 0.03$ , which when translated to  $A_{7\mu\text{m}}/A_K$  lies about 0.1 above the interpolated value of Indebetouw et al. (2005). Flaherty et al. (2007) examined the MIR extinction law toward five nearby star-forming regions using IRAC bands and MIPS  $24\ \mu\text{m}$ . They found that from  $\sim 4\ \mu\text{m}$  to  $8\ \mu\text{m}$  the extinction is also constant but  $A_\lambda/A_{K_s}$  lies systematically above those of Indebetouw et al. (2005) by  $\sim 0.05$  to  $>0.1$ . They suggest that the differences may be due to variation in the diffuse ISM versus molecular cloud extinction laws.

All determinations of the MIR extinction law suffer uncertainties due to uncertain assumptions, location along the line of sight (i.e., different environments), and selection effects introduced by techniques that use different tracers. Even so, there seems to be general agreement that from  $\sim 4\ \mu\text{m}$  to  $8\ \mu\text{m}$  extinction seems to be approximately constant in all environments. There are apparent disagreements about the  $2\text{--}4\ \mu\text{m}$  slope and absolute values of  $A_\lambda/A_K$ . These may be indicative of uncertainties introduced by different techniques or different

environmental conditions. Future studies will be needed to refine the current status of the MIR extinction law.

#### 4. GALACTIC STRUCTURE

As mentioned in § 1, the GLIMPSE surveys have archived over 100 million stars that can be accessed at the Spitzer Science Center archive<sup>12</sup> and eventually at NASA/IPAC Infrared Science Archive (IRSA).<sup>13</sup> The fact that a large number of stars would be detected in the GLIMPSE surveys was understood when the project was proposed, but it was not appreciated how important they would be in tracing large-scale Galactic structure. About 90% of all the stars cataloged are red giants, a good fraction of which appear to be red-clump giants. This is very fortunate because these stars have a small range of intrinsic luminosities, making them good standard candles detectable at MIR wavelengths to large distances.

Let us begin this section with a comparison of the GLIMPSE survey with 2MASS and SDSS. The  $3.6\ \mu\text{m}$  and  $4.5\ \mu\text{m}$  IRAC bands, with sensitivity limits 14.2 and 14.1 mag, respectively (Benjamin et al. 2005), provide the optimum wavelengths for studying Galactic stellar structure. Observations at shorter wavelengths, like the  $2.2\ \mu\text{m}$  K band, are more strongly affected by extinction,  $A_{3.6} \sim 0.6\ A_K \sim 0.06\ A_V$ ; observations at longer wavelengths are comprised of higher levels of diffuse emission from dust and PAH emission, and stellar photospheric fluxes decrease with increasing MIR wavelengths. The 2MASS sensitivity limits in the J, H, K bands are 15.8, 15.1, 14.3 mag, respectively (Skrutskie et al. 2006), slightly fainter than the GLIMPSE sensitivity limits. The distance probed by the two surveys depends on the direction. In low-extinction regions at large Galactic longitudes, 2MASS probes slightly deeper than GLIMPSE; in the inner Galaxy ( $|l| < \sim 40^\circ$ ), GLIMPSE probes deeper than 2MASS because of the lower extinction at GLIMPSE bands. In these regions, however, GLIMPSE is confusion-limited at 13.3–13.6 mag, rather than sensitivity-limited. The SDSS survey, which typically goes to  $\sim 20$  mag, only crosses the Galactic plane in selected directions. Also, because of severe extinction in the optical bands, the SDSS surveys only sample a fairly local volume (radius of a few kpc) toward the region of the inner Galaxy imaged by GLIMPSE.

##### 4.1. The Central Bar

The first indication from GLIMPSE of the Galaxy's central bar is apparent in Figure 10, which clearly shows a strong asymmetry in the number of stars between the first and fourth quadrants of the Galactic plane. There are about 25% more stars per unit area at longitudes from  $0^\circ$  to about  $30^\circ$  than the same

angular interval in the fourth quadrant ( $360^\circ$  to  $330^\circ$ ). An alternative way to show this is to plot the log of the number of stars (per magnitude per square degree) versus magnitude at  $4.5\ \mu\text{m}$ ; such a plot is shown in Figure 12 (from Benjamin et al. 2005). This plot shows that the stellar count at magnitudes from  $\sim 14$  to  $\sim 6.5$  is about the same for lines of sight greater than  $30^\circ$  from the Galactic center, but at  $l = 15.5^\circ$  the number of stars is systematically greater than that at the same distance from the Galactic center at  $l = 344.5^\circ$ . The average slope is about the same for all lines of sight. However, there is a bump at  $\sim 12$ th mag in the curve at  $15.5^\circ$  that does not appear in the line of sight at  $l = 344.5^\circ$ . To investigate the origin of this bump, Benjamin et al. (2005) plotted the power-law exponent of counts as a function of apparent magnitude at  $4.5\ \mu\text{m}$  and Galactic longitude; this plot is shown in Figure 13.

Figure 13 illustrates several important features: (1) along the top at the faintest magnitudes, the confusion limits are apparent; (2) along the lower part of the figure, randomly large departures from the average number count index (slope) occur because of the small number of the brightest stars; (3) from about  $l = 30^\circ$  to  $0^\circ$ , there is a systematic increase in the number count index (this is the steepest part of the bump seen in Fig. 12), and at slightly fainter magnitudes the slope passes through the average slope (*green color*), and then at still fainter magnitudes the slope levels off (*blue to purple colors*); (4) the width of the bump feature in brightness indicates that it traces a stellar population with an intrinsic range of brightness of about 1 mag (i.e., a fairly good standard candle); and (5) the fact that

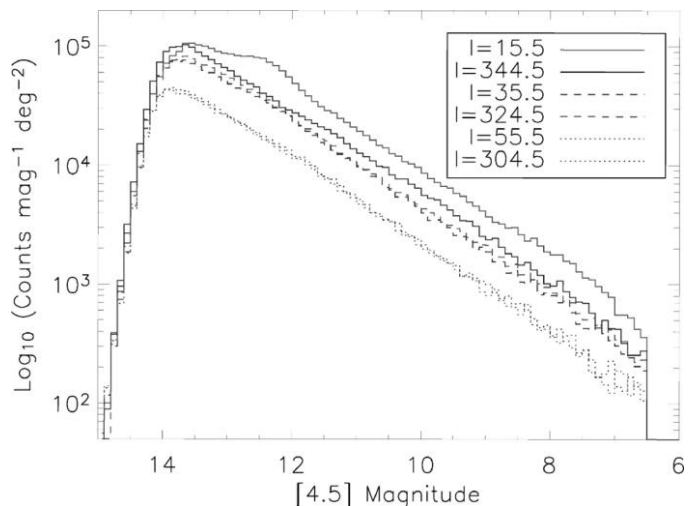


FIG. 12.—Number of sources from the GLMC as a function of magnitude for three pairs of sight lines with members of each pair equidistant from the Galactic center. This is another way of illustrating that the number of sources is the same in the north and south at  $|l| > \sim 30^\circ$  but at  $|l| < \sim 30^\circ$  the number is systematically  $\sim 25\%$  higher in the north than the south at all magnitudes. In addition, there is a hump at  $\sim 12$  mag in the north that is absent in the south; this turns out to be a signature of the northern arm of the central bar (see Benjamin et al. 2005). See the electronic edition of the *PASP* for a color version of this figure.

<sup>12</sup> Find this archive online at <http://ssc.spitzer.caltech.edu/legacy/glimpsehistory.html>.

<sup>13</sup> The NASA/IPAC IRSA is online at <http://irsa.ipac.caltech.edu/data/SPITZER/GLIMPSE>.

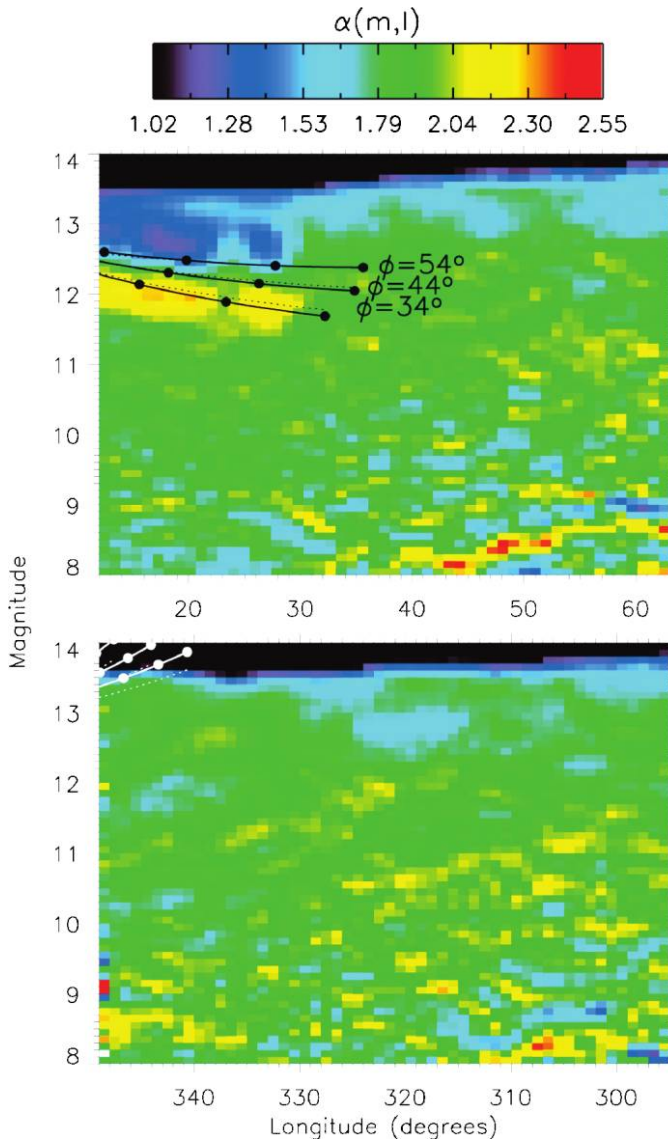


FIG. 13.—Power-law exponent of star counts as a function of apparent magnitude at  $4.5 \mu\text{m}$  and Galactic longitude; this is basically the slope of the curves in Figure 11. The orange-yellow strip at  $\sim 12$ th mag and longitudes  $< 30^\circ$  in the upper panel represents the increase in slope of the hump in Fig. 11; the blue strip is where the slope levels out. This has been modeled by Benjamin et al. (2005) to determine the radius ( $4.4 \pm 0.5$  kpc) and orientation ( $44^\circ \pm 10^\circ$ ) of the bar to the Sun-Galactic center line. The bin size is  $0.1^\circ \times 0.1$  mag.

the bump feature becomes systematically fainter toward the center of the Galaxy implies that the average distance of the tracer increases toward the Galactic center. Benjamin et al. (2005) interpreted Figures 10, 12, and 13 as evidence for a central bar in our Galaxy of radius  $4.4 \pm 0.5$  kpc and oriented about  $44^\circ \pm 10^\circ$  to the Sun-Galactic center line. The central bar is a major feature of our Galaxy. Although not the first to suggest a central bar in our Galaxy, the GLIMPSE data are possibly the strongest evidence for it and certainly the clearest evidence for its extent and orientation.

## 4.2. The Stellar Radial Scale Length

A plot of the number of stars at  $4.5 \mu\text{m}$   $\text{deg}^{-2}$  with longitude shows that the number of stars decrease by a factor of  $\sim 12$  from  $|l| = 10^\circ$  to  $\sim 65^\circ$  and the number versus longitude can be well fit by a first-order modified Bessel function of the second kind (see Fig. 14 and Benjamin et al. 2005), which is expected for an exponential disk. The best-fit curve found by Benjamin et al. (2005) yields an angular radial scale length of  $24.2^\circ \pm 0.3^\circ$ . Assuming the stellar tracers are dominated by red-clump giants, Benjamin et al. (2005) infer that the angular scale length would translate to a linear scale length of  $3.9 \pm 0.6$  kpc. Red-clump giants have a well-established magnitude of  $M_K = -1.62 \pm 0.03$  mag with an intrinsic color of  $(J - K_s)_0 = 0.7$  mag; these values depend weakly on metallicity (Cabrera-Lavers et al. 2007). They also found that the source-count weighted stellar midplane varies by no more than  $\pm 0.05^\circ$  within  $|l| < 65^\circ$  of the Galactic center.

## 4.3. Spiral Arms

Imagine sweeping our line of sight along the Galactic midplane and integrating the number of stars seen along each direction. In this case, at each tangency to a spiral arm, one would expect to see an enhancement of stars because of the increased line of sight path length through the arm and the increased number of stars in the arm. This is, in fact, what one sees with the expected profile of number versus longitude toward the Scutum-

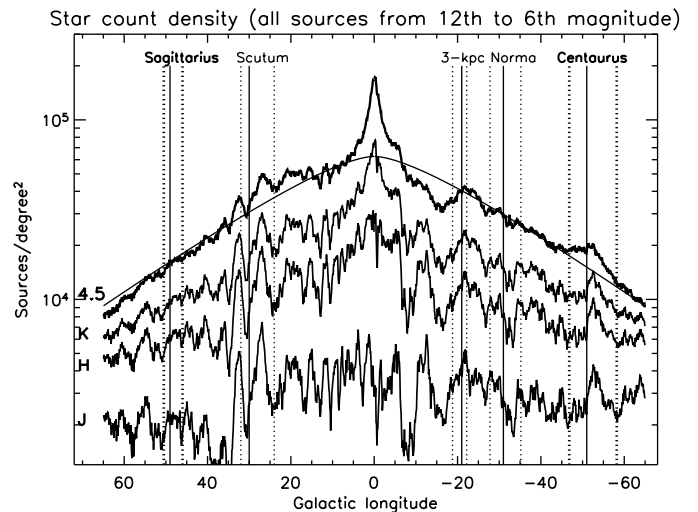


FIG. 14.—Number of sources per  $\text{deg}^2$  as a function of Galactic longitude at  $4.5 \mu\text{m}$ , K, H, and J bands. Many more sources are detected from J to H to K to  $4.5 \mu\text{m}$  due to decreasing extinction. The solid line fit to the  $4.5 \mu\text{m}$  counts is a first-order modified Bessel function of the second kind, which is a good fit at longitudes  $l > 30^\circ$  and  $-20^\circ$  to  $-65^\circ$  (except for the excess at about  $-50^\circ$ , which is the tangency to the Centaurus arm). The large excess at longitudes within about  $5^\circ$ – $6^\circ$  of the Galactic center is due to the nuclear bulge. Note the absence of any indication of a stellar excess at the tangency of the Sagittarius arm.



Centaurus arm tangency at  $306^\circ < l < 313^\circ$  (see Fig. 14). At about the same angular distance from the Galactic center, but on the opposite side ( $\sim 45^\circ < l < \sim 51^\circ$ ), there is no detectable increase in the star count where the Sagittarius arm is expected to lie (see Fig. 14). Although extinction is significantly reduced in the mid-infrared, it is clearly important for selected regions (Benjamin et al. 2005). Combined models of infrared stellar emission and interstellar absorption have been carried out at K band to examine the effect of extinction on the contrast of stellar spiral arm tangencies (Drimmel & Spergel 2001). Models of the effect of lower mid-infrared star counts are currently being developed.

At the 212th American Astronomical Society Meeting in St. Louis, MO, a special two-day meeting on Galactic Spiral Arms took place. At this meeting an attempt was made to visualize the most accurate picture of the Milky Way seen face-on using all available observational data including the stellar data from GLIMPSE, the H I 21 cm Galactic Plane Surveys, and CO surveys. Dame & Thaddeus (2008) reported detection of the counter part of the expanding 3 kpc arm lying on the far side of the Galactic center, a feature predicted by Oort (1964) but only established in 2008. The best visualization of the face-on Milky Way constrained by the currently available data, shown in Figures 15 and 16, was constructed by R. Hurt of the Spitzer Space Science Center in consultation with R. Benjamin of the University of Wisconsin-Whitewater. Figure 16 is an annotated version of Figure 15.

Figures 15 and 16 are an attempt to synthesize over a half-century of work on Galactic structure by many authors. Some of the key elements taken into account in constructing Figures 15 and 16 are briefly discussed in the following.

*Distance to the Galactic center.*—All results have been scaled to a fiducial distance to the Galactic center of  $R_{GC} = 8$  kpc (Reid 1993), somewhat less than the standard IAU distance of  $R_{GC} = 8.5$  kpc (Kerr & Lynden-Bell 1986). Analysis of the S2 stellar orbit around Sag A\* (Eisenhauer et al. 2005), indicates an even shorter distance of  $R_{GC} = 7.62$  kpc with a statistical uncertainty of  $\pm 0.32$  kpc and a systematic uncertainty of  $\pm 0.16$  kpc, a result that has yet to be confirmed by an independent analysis.

*Galactic Bar.*—The parameters of the Galactic stellar bar, also referred to as the COBE/DIRBE bar, the triaxial bulge, or the bulgey-bar, have principally been constrained by analysis of near- and mid-IR low-resolution images and also microlensing studies toward low-extinction windows, and has been reviewed by Gerhard (2002) and Merrifield (2004). Gerhard adopts an aspect ratio of 10:4:3 (length:width:height), a half-length of  $\sim 3.1$ – $3.5$  kpc, and an angle of  $\Phi = 20^\circ$  with respect to the Galactic Center-Sun line, where  $\Phi = 0 - 90^\circ$  puts the near end of the bar in the first quadrant  $l = 0 - 90^\circ$  of the Galactic plane. This structure is much more vertically extended than the thin stellar disk.

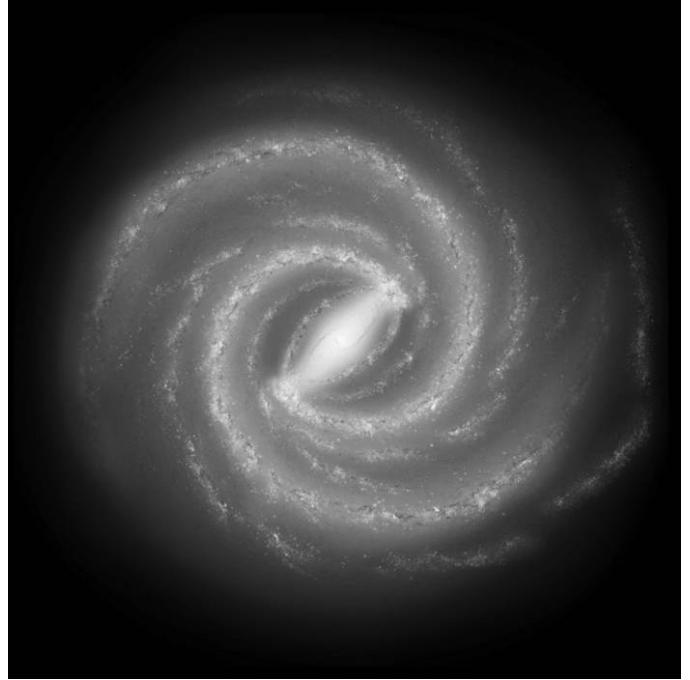


FIG. 15.—Sketch of approximately how the Galaxy is likely to appear viewed face-on. This sketch was made by Robert Hurt of the Spitzer Science Center in consultation with Robert Benjamin at the University of Wisconsin-Whitewater. The image is based on data obtained from the literature at radio, infrared, and visible wavelengths. As viewed from a great distance our Galaxy would appear to be a grand-design two-armed barred spiral with several secondary arms: the main arms being the Scutum-Centaurus and Perseus arms and the secondary arms being Sagittarius, the outer arm, and the 3 kpc expanding arm (see Fig. 14). See the electronic edition of the *PASP* for a color version of this figure.

*Long Bar.*—Several studies of near-infrared selected red-clump giants in the midplane have indicated a *second* non-axisymmetric structure in the inner Galaxy, which is vertically thinner than the COBE/DIRBE bar. First claimed by Hammersley et al. (2000), this “Long Bar” was confirmed independently with GLIMPSE data. The dynamical relation between the two bars is still unclear.

*Near and Far 3-kpc Arms.*—Neutral hydrogen 21-cm surveys discovered the “Expanding 3-kpc Arm,” named for its angular size and approaching Doppler shift for gas in the direction  $l = 0^\circ$  (van Woerden 1957). It is now generally thought to be associated with gas flow roughly parallel to the bar. The far-side counterpart was recently discovered by Dame & Thaddeus (2008). Placement of this gas on an image requires combining CO and H I position-velocity data with a dynamical model of gas flow in a barred potential. The model of Fux (1999) was used. This model was also used to assign a position to the dust-lanes of the bar and the Central Molecular Zone (Morris & Serabyn 1996).

*Outer Spiral Arms.*—Outside the zone of influence of the bar, it is generally, but provisionally, assumed that the Galaxy has four principal spiral arms: Norma, Sagittarius, Perseus, and

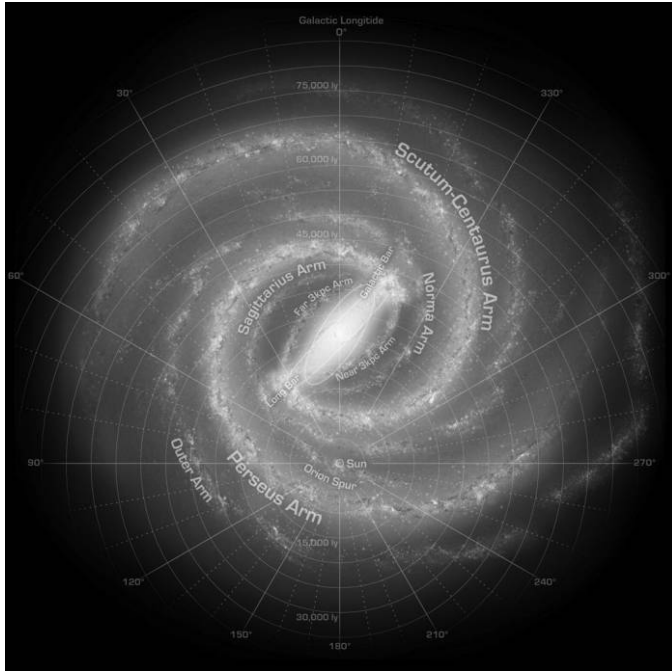


FIG. 16.—This is the same image as Fig. 15 with Galactic coordinates overlaid and the locations of spiral arms and the Sun indicated. See the electronic edition of the *PASP* for a color version of this figure.

Scutum-Centaurus. (The final arm is also referred to as Scutum-Crux, but the tangency direction of this arm is clearly in the constellation Centaurus.) The most commonly adopted model originates with the H II region study of Georgelin & Georgelin (1976). There have been many other models proposed (Liszt 1985); numerous variations persist to this day. The image shown continues the tradition of using the Georgelin & Georgelin model as the template, with (1) tweaks in positions to incorporate the results of Very Long Baseline Array (VLBA) parallax distances to masers in selected star-formation regions, c.f. Xu et al. (2006), (2) refined spiral arm tangency directions from CO surveys (Dame et al. 2001), and (3) revised “amplitudes” of the arms to reflect evidence that the Scutum-Centaurus and Perseus arms are associated with overdensities in the old stellar disk, but the Norma and Sagittarius arms are not. This final modification is based on GLIMPSE results as well as work by Drimmel (2000) and Drimmel & Spergel (2001). Of all the elements of Figure 15 and 16, the spiral structure is still the most problematic and deserves much more attention from the community. The image also shows the placement of the “Outer” and “Distant” spiral arm(s), which have been placed kinematically as in McClure-Griffiths et al. (2004).

## 5. EVOLVED STARS

Robitaille et al. (2008) have identified  $\sim 7500$  IR-selected AGB stars in the GLIMPSE survey. Due to the red color selections, most of the AGB stars are extreme AGBs. Prior to this,

most known AGB stars in our Galaxy were nearby ( $<1$  kpc), optically selected sources, most of which saturate in the GLIMPSE survey. The Robitaille et al. selection represents a newly discovered population of AGB stars distributed throughout the Galaxy. By comparing GLIMPSE and *MSX* catalogs, taken nearly a decade apart, Robitaille et al. (2007) identified over 500 highly variable sources, most of which are likely to be evolved (AGB) stars. Together, these catalogs provide a rich data set for follow-up by the evolved star community. A few of the PNe identified by Kwok et al. (2008) appear to be compact H II regions (Y.-H. Chu private communication, 2009).

Cohen et al. (2005) reported on the Planetary nebula, G313.3 + 00.3, discovered from radio and GLIMPSE observations. Cohen et al. (2007) analyzed 58 PNe, comparing optical and MIR (3.6–8.0  $\mu\text{m}$ ) morphologies and MIR and radio fluxes to discriminate between thermal and nonthermal emission. Kwok et al. (2008) located 30 PNe in the GLIMPSE survey and analyzed their IR SEDs. They were able to separate photospheric, nebular, and dust emission components.

Reach et al. (2006) searched 99 known super nova remnants (SNRs) and detected 18 in the GLIMPSE I survey area. The bright diffuse background emission in the Galactic plane coupled with the faintness of IR emission in IRAC bands by SNRs probably limited the number of detections.

## 6. SERENDIPITY

The GLIMPSE surveys have been a rich source of serendipitous discoveries. In a sense the discovery of EGOs, large-scale Galactic structure traced by the old population of K and ME giant stars, triggered star formation associated with expanding bubbles, the prevalence of bow shocks in massive star-formation regions, and dust emission properties are serendipitous. Although not a serendipitous discovery, Kobulnicky et al. (2005) reported a globular cluster located in the Galactic plane (i.e. the “zone of avoidance”) at  $l = 31^\circ$ ,  $b = -0.1^\circ$ , which at its estimated distance would be the brightest cluster as observed from the Earth except for the fact that it is attenuated by  $A_V \sim 15$  mag. This cluster was just barely detected in 2MASS (Simpson & Cotera 2004), but in the IRAC bands it is very obvious. Close to a dozen galaxies in the Great Attractor cluster were detected through the foreground Galactic haze (two of which have been confirmed spectroscopically by Jarrett et al. 2007). Mercer et al. (2007) reported detection of a curious object that they call the “Southern Jellyfish Nebula.” This object has mid-IR filaments or “ropes of nebular emission” with length-to-width ratios  $>20:1$ , the nature of which is not known. They suggest the following possible explanations for the appearance of the rope pattern: (1) confinement of matter by magnetic fields; (2) formation via instabilities; (3) illumination of scattering surfaces; (4) excitation of spectral line emission features; and (5) projection effects. They mention that this object does not appear to be unique and reference several other similar objects. Finally, the discovery that YSOs are distributed

throughout molecular clouds, not just toward the centers of H II regions, was unanticipated by many in the star-formation community.

## 7. SUMMARY

A brief summary is given of some of the main contributions enabled by the GLIMPSE surveys. This includes contributions to star formation and early stages of evolution, in particular the morphologies and properties of IRDCs, EGOs and other YSOs, and mid-infrared bubbles and H II regions. Over 30 new  $\beta$  Pic candidates have been identified via their MIR excess emission. Large-scale Galactic structure as traced by the distribution of red giants has clearly revealed the radius and orientation of the central bar, the tangency to the Scutum-Centaurus arm, no such tangency toward the Sagittarius arm, and the stellar radial scale length. It now appears that the Milky Way is a barred, grand-design two-armed spiral with at least two secondary arms (the Sagittarius and Norma arms). The distribution and ubiquity of dust and PAHs in the interstellar medium are highlighted by the GLIMPSE images, as are the prevalence of bow shocks, pillars, and instabilities in massive star-formation regions.

As of 2008 November, we are aware of at least 70 publications that have used GLIMPSE data. This is undoubtedly a lower limit because we do not survey all journals. The GLIMPSE images and point-source lists GLMC and GLMA provide a rich scientific database whose potential has only begun to be tapped.

Future systematic analyses of the GLIMPSE data are likely to be its greatest value to the community. We also expect strong synergies with upcoming surveys of the Galactic plane. It is highly likely that the GLIMPSE images and point-source archive will be used for investigations well beyond any imagined by those of us involved with planning and executing the program. We wish them good hunting.

We wish to acknowledge an anonymous referee who made numerous suggestions that have significantly improved and expanded this presentation. We thank the entire GLIMPSE team, all of whom have contributed to the success of the GLIMPSE project. Of course none of this would have been possible without the strong support of the Spitzer Science Center personnel from whom we had excellent support. We acknowledge Giovanni Fazio and his team who built the IRAC instrument, and those who designed, built, and launched the *Spitzer* satellite. A special acknowledgment to Tom Soifer and Mike Werner who have insisted on high standards for the *Spitzer* mission. We would like to acknowledge Claudia Cyganowski for providing Fig. 5, Steve Bracker for Fig. 6, Thomas Robitaille for Fig. 7, Christer Watson for Fig. 9, Matt Povich for Fig. 11, Bob Benjamin for Figs. 10, 12, 13, and 14, and Robert Hurt of the Spitzer Science Center for Figs. 15 and 16. We acknowledge support from the following NASA/JPL contracts: 1224653, 1275394, 1282620, 1289524, and 1298148.

## REFERENCES

- Allen, L., et al. 2007, in *Protostars & Planets V*, eds. B. Reipurth, D. Jewitt, & K. Keil (Tucson: Univ. Arizona Press), 361–376
- Benjamin, R. A., et al. 2005, *ApJL*, 630, L149
- Bergin, E. A., & Tafalla, M. 2007, *ARA&A*, 45, 339
- Bethell, T. J., Zweibel, E. G., & Li, P. S. 2007, *ApJ*, 667, 275
- Cabrera-Lavers, A., et al. 2007, *A&A*, 465, 825
- Carey, S. J. 2008, *BAAS*, 40, 255
- Carey, S. J., et al. 1998, *ApJ*, 508, 721
- Caswell, J. L. 1996, *MNRAS*, 279, 79
- Churchwell, E., & Everett, J. E. 2008, Presentation at The Birth and Feedback of Massive Stars Within and Beyond the Galaxy (Charlottesville, VA), <http://www.cv.nrao.edu/php/meetings/massive08/program.shtml>
- Churchwell, E., et al. 2004, *ApJS*, 154, 322
- . 2006, *ApJ*, 649, 759
- . 2007, *ApJ*, 670, 428
- Cohen, M., et al. 2005, *ApJ*, 627, 446
- . 2007, *ApJ*, 669, 343
- Cox, A. N. 2000, *Allen's Astrophysical Quantities*, (4th ed.; New York: AIP Press Springer), 572
- Cragg, D. M., Sobolev, A. M., & Godfrey, P. D. 2005, *MNRAS*, 360, 533
- Cyganowski, C., et al. 2008, *AJ*, 136, 2391
- Dame, T. M., Hartmann, D., & Thaddeus, P. 2001, *ApJ*, 547, 792
- Dame, T. M., & Thaddeus, P. 2008, *ApJL*, 683, L143
- Davis, C. J., Kumar, M. S. N., Sandell, G., Froebrich, D., Smith, M. D., & Currie, M. J. 2007, *MNRAS*, 374, 29
- Devharveng, L., Zavagno, A., & Caplan, J. 2005, *A&A*, 433, 565
- Devine, K., et al. 2009, *ApJ*, submitted
- Draine, B. T. 2003, *ARA&A*, 41, 241
- Drimmel, R. 2000, *A&A*, 358, L13
- Drimmel, R., & Spergel, D. N. 2001, *ApJ*, 556, 181
- Egan, M. P., et al. 1998, *ApJL*, 494, L199
- Eisenhauer, F., et al. 2005, *ApJ*, 628, 246
- Ellingsen, S. P. 2006, *ApJ*, 638, 241
- . 2007, *MNRAS*, 377, 571
- Fazio, G. G., et al. 2004, *ApJS*, 154, 10
- Flaherty, K. M., et al. 2007, *ApJ*, 663, 1069
- Frieswijk, W. F., et al. 2008, *ApJ*, 685, L51
- Fux, R. 1999, *A&A*, 345, 787
- Ganesh, S., et al. 2008, *A&A*, in press (astro-ph 0809.1741)
- Georgelin, Y. M., & Georgelin, Y. P. 1976, *AAp*, 49, 57
- Gerhard, O. 2002, ASP Conf. Ser. 273, *The Dynamics, Structure & History of Galaxies*, ed. G. S. Da Costa, & H. Jerjen (San Francisco: ASP), 73
- Gutermuth, R. A., et al. 2004, *ApJS*, 154, 374
- . 2005, *ApJ*, 632, 397
- . 2008, *ApJ*, 673, L151
- Hammersley, P. L., Garzón, F., Mahoney, T. J., López-Corredoira, M., & Torres, M. 2000, *MNRAS*, 317, L45



- Helfand, D. J., Becker, R. H., White, R. L., Fallon, A., & Tuttle, S. 2006, *AJ*, 131, 2525
- Hennebelle, P., Péroult, M., Teyssier, D., & Ganesh, S. 2001, *A&A*, 365, 598
- Heitsch, F., et al. 2007, *ApJ*, 656, 227
- Indebetouw, R., et al. 2005, *ApJ*, 619, 931
- Indebetouw, R., et al. 2007, *ApJ*, 666, 321
- Jarrett, T. H., et al. 2007, *AJ*, 133, 979
- Jiang, B. W., Omont, A., Ganesh, S., Simon, G., & Schuller, F. 2003, *A&A*, 400, 903
- Kerr, F. J., & Lynden-Bell, D. 1986, *MNRAS*, 221, 1023
- Kessler, M. F., et al. 1996, *A&A*, 315, L27
- Kobulnicky, H. A., et al. 2005, *AJ*, 129, 239
- Kwok, S., Koning, N., Huang, H.-H., & Churchwell, E. 2008, *ApJS*, 174, 426
- Lamers, H. J. G. L. M., & Cassinelli, J. P. 1999, *Introduction to Stellar Winds*, (Cambridge, UK: Cambridge Press)
- Liszt, H. S. 1985, *IAU Symposium 106, The Milky Way Galaxy*, ed. H. van Woerden, R. J. Allen, & W. B. Burton (Dordrecht: Reidel Publishing Company), 283
- Lutz, D., et al. 1996, *A&A*, 315, L269
- Marston, A. P., et al. 2004, *ApJS*, 154, 333
- McClure-Griffiths, N. M., Dickey, J. M., Gaensler, B. M., & Green, A. J. 2004, *ApJL*, 607, L127
- Megeath, S. T., et al. 2004, *ApJS*, 154, 367
- Menten, K. M., Pillai, T., & Wyrowski, F. 2005 in *IAU Symp. 227, Massive Star Birth: A Crossroads of Astrophysics*, ed. R. Cesaroni et al. (Cambridge: Cambridge Univ. Press), 23
- Mercer, E. P. 2007, *ApJ*, 656, 242
- Mercer, E. P., et al. 2005, *ApJ*, 635, 560
- Merrifield, M. R. 2004, *ASP Conf. Ser. 317, Milky Way Surveys: The Structure and Evolution of Our Galaxy*, ed. D. Clemens, R. Y. Shah, & T. Brainerd (San Francisco: ASP), 289
- Minier, V., Ellingsen, S. P., Norris, R. P., & Booth, R. S. 2003, *A&A*, 403, 1095
- Morris, M., & Serabyn, E. 1999, *ARAA*, 34, 645
- Muzerolle, J., et al. 2004, *ApJS*, 154, 379
- Noreiga-Crespo, A., et al. 2004, *ApJS*, 154, 352
- Oort, J. H. 1964, *IAU Symp. 20, The Galaxy and Magellanic Clouds*, ed. J. Kerr, & A. . Rodgers (Canberra: Australian Acad. Science), 1
- Pillai, T., et al. 2006, *A&A*, 447, 929
- . 2007, *A&A*, 467, 207
- Povich, M. S., et al. 2007, *ApJ*, 660, 346
- . 2008, *ApJ*, 689, 242
- . 2009, *ApJ*, submitted
- Price, S. D., Egan, M. P., Carey, S. J., Mizuno, D. R., & Kuchar, T. A. 2001, *AJ*, 121, 2819
- Ragan 2006, *ApJS*, 166, 567
- Rathborne, J. M., Jackson, J. M., & Simon, R. 2006, *ApJ*, 641, 389
- Rathborne, J. M., et al. 2005, *ApJL*, 630, L181
- Reach, W. T., et al. 2006, *AJ*, 131, 1479
- Redman, R. O., et al. 2003, *ApJ*, 586, 1127
- Reid, M. J. 1993, *ARAA*, 31, 345
- Rieke, G. H. 2004, *ApJS*, 154, 25
- Robitaille, T. P., Whitney, B. A., Indebetouw, R., & Wood, K. 2007, *ApJS*, 169, 328
- Robitaille, T. P., Whitney, B. A., Indebetouw, R., Wood, K., & Denzmore, P. 2006, *ApJS*, 167, 256
- Robitaille, T. P., et al. 2008, *AJ*, 136, 2413
- Roman-Zúñiga, C. G., Lada, C. J., Muench, A., & Alves, J. F. 2007, *ApJ*, 664, 357
- Sakai, T., et al. 2008 *ApJ*, 678, 1049
- Shepherd, D. S., et al. 2007, *ApJ*, 669, 464
- Simon, R., et al. 2006, *ApJ*, 653, 1325
- Simpson, J. P., & Cotera, A. S. 2004, Poster at AAS 204th Meeting, Denver, Session 45.01
- Skrutskie, M. F., et al. 2006, *AJ*, 131, 1163
- Smith, H. A., Hora, J. L., Marengo, M., & Pipher, J. L. 2006, *ApJ*, 645, 1264
- Smith, M. D., & Rosen, A. 2005, *MNRAS*, 357, 1370
- Szymczak, M., Pillai, T., & Menten, K. M. 2005, *A&A*, 434, 613
- Uzpen, B., et al. 2005, *ApJ*, 629, 512
- . 2007, *ApJ*, 658, 1264
- van Woerden, H., Rougoor, G. W., & Oort, J. H. 1957, *CR Acad. Sci. Paris*, 244, 1691
- Velusamy, T., Langer, W. D., & Marsh, K. A. 2007, *ApJ*, 668, L159
- Walsh, A. J., Burton, M. G., Hyland, A. R., & Robinson, G. 1998, *MNRAS*, 301, 640
- Wang, Y., et al. 2008, *ApJL*, 672, L33
- Watson, C., et al. 2008, *ApJ*, 681, 1341
- Weaver, R., McCray, R., Castor, J., Shapiro, P., & Moore, R. 1977, *ApJ*, 218, 377
- Werner, M. W., et al. 2004, *ApJS*, 154, 1
- Whitney, B. A., Indebetouw, R., Bjorkman, J. E., & Wood, K. 2004a, *ApJ*, 617, 1177
- Whitney, B. A., Wood, K., Bjorkman, J. E., & Cohen, M. 2003b, *ApJ*, 598, 1079
- Whitney, B. A., Wood, K., Bjorkman, J. E., & Wolff, M. J. 2003a, *ApJ*, 591, 1049
- Whitney, B. A., et al. 2004b, *ApJS*, 154, 315
- Whittet, D. C. B. 1992, *Dust in the Galactic Environment*, in *The Graduate Series in Astronomy*, eds. Taylor, & R. E. White (Philadelphia: Inst. Physics Pub., Bristol)
- Xu, Y., Reid, M. J., Zheng, X. W., & Menten, K. M. 2006, *Science*, 311, 54
- Yusef-Zadeh, F., et al. 2007, *IAU Symp. 242, Astrophysical Masers & their Environments*, ed. J. M. Chapman, & W. A. Baan (Cambridge: Cambridge Univ. Press), 366